Δ excitations in nuclei and their decay properties

T. Udagawa
Department of Physics, University of Texas, Austin, Texas 78712

P. Oltmanns and F. Osterfeld
Institut für Kernphysik, KFA Jülich GmbH, 52425 Jülich, Germany

S. W. Hong
Sung Kyun Kwan University, Suwon, 440-746, Korea
(Received 18 October 1993)

A formalism for the calculation of intermediate energy charge exchange reactions exciting the Δ resonance region in nuclei is presented. The nuclear structure part of the formalism is based on the isobar-hole model and the nuclear reaction part is treated within the distorted-wave impulse approximation (DWIA). In the nuclear structure part, all important nuclear medium effects are included, such as nucleon and isobar binding, two-body Δ isobar-nucleon hole correlations, and intermediate coupling to multiparticle-multihole channels. The latter coupling is treated phenomenologically through a Δ spreading potential. Explicit account is also taken of the nucleon knockout mode and the related nucleon particle-nucleon hole correlations. In order to perform the calculations, we first set up coupled-channel equations for the excited nucleon and Δ, which are slightly, but importantly, transformed into equations for localized functions only. We solve these equations by using the Lanczos method. The resultant formalism allows us to calculate cross sections for Δ excitation, quasielastic scattering, and low-lying Gamow-Teller excitations on the same footing. In this way a detailed study of the nuclear medium effects on the Δ isobar can be done. Particular attention is paid to the Δ-hole correlations in the spin-longitudinal ($\mathbf{S}\cdot\mathbf{q}\ \mathbf{T}$) channel. It is shown that the coherent pion production events in the exclusive ^{12}C$(p,n\pi^+)^{12}$C(g.s.) and ^{12}C$(^3$He$,t\pi^+)^{12}$C(g.s.) reactions provide a unique signature on the nuclear pionic mode.

PACS number(s): 14.20.Gk, 21.10.Re, 24.30.Cz

I. INTRODUCTION

The most important and widely publicized issue in the study of intermediate energy charge exchange reactions is the downward energy shift of the Δ resonance peak position by ~ 70 MeV in nuclear targets as compared to the proton target [1–7]. The physical significance of this shift was first recognized by Contardo *et al.* [2] in their studies of the (^{3}He,t) reaction at the Laboratoire National Saturne in Paris. The phenomenon, however, is also found to persist in other charge exchange reactions, such as the (p,n) reaction at E=800 MeV [4–7]. In Fig. 1 we show an experimental zero-degree spectrum for the $p(p,n)\Delta^{++}$ reaction [3] at E=800 MeV incident energy in comparison with a corresponding one of the ^{12}C(p,n) reaction [5]. The spectra are plotted versus the excitation energy ω_L in the laboratory (L) system. A considerable energy shift of ~ 70 MeV is observed between the elementary Δ excitation of the proton and the Δ excitation in ^{12}C. For the proton target the Δ resonance peak position appears at ω_L ~365 MeV while for the ^{12}C target the peak appears at ω_L ~ 295 MeV. The peak position for the proton target can be explained by the sum of the Δ resonance excitation energy ω_R=295 MeV and the recoil energy of ~95 MeV received by the Δ^{++} in the (p,n) excitation process. The small energy difference of ~ −25 MeV between the sum of the two energies (390 MeV) and the observed energy (365 MeV) can be ascribed to the momentum transfer dependence of the form factors involved in the $p+p\rightarrow n+\Delta^{++}$ transition operator.

The shift of the Δ peak position, as observed in Fig. 1, has various origins. The most important one is the Fermi motion (binding) of the nucleons and of the Δ isobar in the nuclear mean field [8,9]. Other, smaller effects come from Δ conversion processes, such as $\Delta+N\rightarrow N+N$

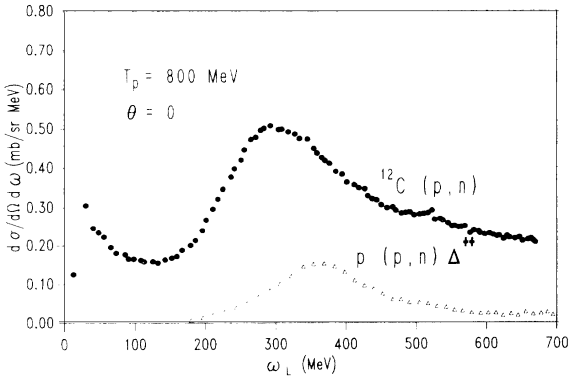

FIG. 1. Experimental zero-degree spectra of the ^{12}C(p,n) reaction [5] in comparison with the $p(p,n)\Delta^{++}$ reaction [3] at E =800 MeV.

[10–12], and from projectile excitation [13,14]. These effects together account for ~ 40 MeV of the shift, leaving 30 MeV unexplained. This latter part of the shift is thought to be due to a nuclear medium correlation effect on the spin-longitudinal response function [10,11,15–18]. In particular, recent calculations of Delorme and Guichon [10] and Udagawa *et al.* [11] performed for finite nuclei consistently show that this second part of the shift is caused by the energy (ω) dependent π-exchange interaction in the nuclear medium. The π exchange provides a strongly attractive interaction between Δ-particle nucleon-hole (ΔN^{-1}) states in the spin-longitudinal ($\mathbf{S}\cdot\mathbf{q}\,\mathbf{T}$) channel leading to a collective pionic mode in the nucleus at lower excitation energies of $\omega_L \sim 250$ MeV.

The inclusive charge exchange cross sections contain information on both the spin-transverse (TR) and the spin-longitudinal (LO) nuclear response functions. The two responses can be experimentally separated either by performing complete spin-flip transfer experiments [19] or by measuring the pion decay of the Δ resonance in coincidence with the ejectile [20–26]. In this paper we shall show that in particular, the coherent pion decay is very sensitive to the LO response function. We remark that the TR and LO spin responses can be experimentally separated by using other probes, such as photon-nucleus and pion-nucleus scattering. The photon is a purely spin-transverse ($\mathbf{S}\times\mathbf{q}\,\mathbf{T}$) probe while the pion is a purely spin-longitudinal probe. Indeed, a shift of the Δ peak position has been observed in π-nucleus total and elastic scattering cross sections [27–29]. In contrast to this, in the case of γ absorption [29,30] and inelastic electron scattering experiments [31–33] the Δ peak does not show such a pronounced displacement.

The aim of this paper is twofold. First, we present a detailed account of the formulation and methods of calculation used in the analysis of the data. This formulation is given in Sec. II. Second, we present results of numerical calculations in a more systematic manner than we did before in our short Letters [11,23]. We shall also discuss various new aspects of the nuclear medium effect, the central issue of the present work.

In Sec. II we first summarize the basic model assumptions made throughout the present paper and state the model Hamiltonian. The nuclear structure part of the model is based on the isobar model [27–29,34] and the nuclear reaction part is treated within the distorted-wave impulse approximation (DWIA) [35]. In the nuclear structure part, all important nuclear medium effects, such as the Δ mean field effects, the Δ spreading potential, and the two-body Δ-hole correlations, are taken into account. In addition, the nucleon knockout effects are included explicitly, so that the resultant formalism allows us to calculate cross sections for Δ excitations and quasielastic charge exchange scattering on the same footing. For that purpose, we first set up a set of coupled-channel equations for the excited nucleon and Δ, respectively. This set is slightly, but importantly, transformed into equations for localized functions. We then apply the Lanczos method for solving the equations. We split the calculated inclusive cross section into its various partial cross sections, as there are the coherent pion production cross section, the quasifree decay, the spreading cross section, and the nucleon knockout and nucleon knockout-fusion cross sections.

In Sec. III we first discuss the parameters used in the present calculations. Then we present the results of our cross section calculations and compare them to the experimental data. We also make various studies of the nuclear medium effect on the Δ with a special emphasis on the Δ-hole correlations in the spin-longitudinal channel. Finally, in Sec. IV we give a summary and conclusions.

II. THEORY

We are interested here in the calculation of the inclusive cross sections for intermediate energy charge exchange reactions, such as $A(p,n)$, $B(d,2p)$, or $C(^3\mathrm{He},t)$. Since we shall deal with high incident projectile energies ($E_{\mathrm{proj}} > 650$ MeV/nucleon), we assume that the impulse approximation is valid and that the cross section can be calculated within the DWIA [35]. We have to keep in mind, however, that the scattering data which we analyze in this paper involve large momentum transfers ($q \sim 2$ fm^{-1}). Therefore two-step processes can still give a significant contribution to the cross section.

A. The distorted-wave impulse approximation

We start our formulation writing down the double differential cross section for the inclusive charge exchange process $A + a \to B + b$, where A (B) and a (b) represent the target (residual nucleus) and projectile (ejectile), respectively (see Fig. 2). In the reaction a particle-hole (ph) state is created in the residual nucleus B, where the particle p can be either a Δ or a nucleon N. Using relativistic kinematics the cross section in the Breit frame of the target system is given as

$$\frac{d^2\sigma}{dE_b d\Omega_b} = \frac{E_A E_a E_B E_b}{2\pi^2\sqrt{\lambda(s,M_a^2,M_A^2)}}\frac{p_b}{E_B}\frac{M_a}{E_a}\frac{M_b}{E_b} \times\overline{\sum}\,|\,T_{\beta\alpha}\,|^2\,\delta(E_B+E_b-E_A-E_a), \tag{1}$$

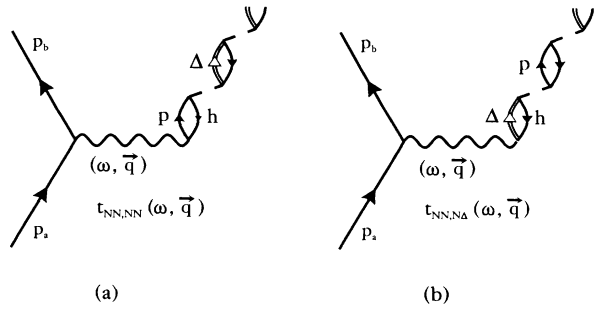

FIG. 2. Graphical representation of reaction processes included in the distorted-wave impulse approximation calculations. For the effective projectile–target nucleon interaction the free $t_{NN,NN}$ matrix is used (a) and for the projectile-isobar coupling the $t_{NN,N\Delta}$ interaction of Eq. (10) is used (b).

where $E_i = \sqrt{M_i^2 + p_i^2}$ is the total energy of particle i ($i = A, B, a, b$), M_i is its rest mass, and p_i is its momentum. (We use natural units throughout, i.e., $\hbar = c = 1$.) An average over the initial spin orientations and a sum over the final spin orientations of both the projectile and the target spin states are taken.

In first order DWIA the transition amplitude $T_{\beta\alpha}$ corresponding to the graphs in Fig. 2 is given as

$$T_{\beta\alpha}^{\rm DW} = \int d\mathbf{R}\chi_b^{(-)^*}(\mathbf{k}_b, \mathbf{R})\langle\Phi_B\Phi_b \mid \times \sum_{\substack{j=1,A \\ i=1,a}} t_{ij} \mid \Phi_A\Phi_a\rangle\chi_a^{(+)}(\mathbf{k}_a, \mathbf{R}), \quad (2)$$

where the initial and final nuclear states of the projectile and target are denoted by $\mid \Phi_a\rangle$,$\mid \Phi_b\rangle$ and $\mid \Phi_A\rangle$, $\mid \Phi_B\rangle$, respectively. The indices A, B, a, and b represent all quantum numbers necessary for specifying the corresponding state, including the spin and isospin quantum numbers. For the intrinsic projectile (ejectile) wave function $\mid \Phi_a\rangle$ ($\mid \Phi_b\rangle$) we use the simple product form, i.e., $\mid \Phi_a\rangle = \mid \phi_a\rangle \mid \phi_{s_a m_a \nu_a}\rangle$, where $\mid \phi_a\rangle$ and $\mid \phi_{s_a m_a \nu_a}\rangle$ are the space part and the spin-isospin part of the wave function, respectively; ν_a denotes the isospin projection. As usual, $\chi_a^{(+)}$ and $\chi_b^{(-)^*}$ are the optical model wave functions of the projectile and ejectile in the initial and final channels. They are functions of the relative coordinate $\mathbf{R}$ between the center of mass of the projectile and the target. Because of the high incident energies we neglect the spin-orbit interaction in the distortion. The transition amplitude of Eq. (2) is evaluated in the Breit frame of the target system. In this system the state of the nucleus is well described by an ordinary nonrelativistic wave function.

In Eq. (2), t_{ij} is the effective interaction between the projectile nucleon i and the target nucleon j. The t_{ij} is represented by the free nucleon-nucleon $t_{NN,NN}$ matrix in the case of the nucleon excitation [Fig. 2(a)] while it is approximated by the free nucleon-nucleon $NN \to N\Delta$ transition operator $t_{NN,N\Delta}$ for the Δ excitation. We shall discuss the specific form of the interaction later. For the moment we just take advantage of the fact that at high incident energies and large momentum transfers both interactions turn out to be rather short ranged, i.e., very weakly dependent on the four-momentum transfer $(\omega, \mathbf{q})$ [$\equiv (E_a - E_b, \mathbf{p}_a - \mathbf{p}_b)$]. Therefore they can be well approximated by local operators in r space of essentially δ-function form. We shall show later the consequences of the short rangeness of the interaction for nucleon-induced reactions. In the case of nucleon-nucleus scattering the effective interaction depends on the relative distance $\mathbf{r}_{0j} = \mathbf{r}_0 - \mathbf{r}_j$ between the projectile 0 and the target nucleon j. Then we express $t_{0j}(\omega, \mathbf{r}_0 - \mathbf{r}_j)$ in terms of its Fourier components $t_{0j}(\omega, \mathbf{q}\,')$,

$$t_{0j}(\omega, \mathbf{r}_0 - \mathbf{r}_j) = \frac{1}{(2\pi)^3}\int d\mathbf{q}\,' \exp[i\mathbf{q}\,' \cdot (\mathbf{r}_0 - \mathbf{r}_j)]t_{0j}(\omega, \mathbf{q}\,'), \quad (3)$$

and use the fact that $t_{0j}(\omega, \mathbf{q}\,')$ is only weakly momentum dependent in the four-momentum transfer region of interest. Then we may approximate Eq. (3) by

$$t_{0j}(\omega, \mathbf{r}_0 - \mathbf{r}_j) \approx t_{0j}(\omega, \mathbf{q})\frac{1}{(2\pi)^3}\int d\mathbf{q}\,' \exp[i\mathbf{q}\,' \cdot (\mathbf{r}_0 - \mathbf{r}_j)] = t_{0j}(\omega, \mathbf{q}\,)\delta^3(\mathbf{r}_0 - \mathbf{r}_j), \quad (4)$$

where $(\omega, \mathbf{q}\,)$ is the four-momentum transfer of the reaction.

If the projectile is a composite particle, we have to take into account the finite size effect of the projectile by using the projectile transition density ρ_{ba}. In a high energy approximation for t_{ij}, as in Eq. (4), this effect can be included by means of the Fourier transform of ρ_{ba} written in a Lorentz invariant form as $f_{ba}(\sqrt{-t})$. This Fourier transform is most conveniently performed in the Breit frame of the projectile since in this frame the wave functions of the projectile and ejectile can be described by nonrelativistic wave functions [36]. We may then write

$$(\phi_b \mid t_{ij} \mid \phi_a) \approx f_{ba}(\sqrt{-t})t_{ij}(\omega, \mathbf{q}\,)\delta^3(\mathbf{R} - \mathbf{r_j}). \quad (5)$$

Here $f_{ba}(\sqrt{-t})$ is the projectile transition form factor in momentum representation. It is a function of the square of the four-momentum transfer $t \equiv \omega^2 - \mathbf{q}^{\,2}$. Note that Eq. (5) is also valid for nucleon-nucleus scattering if one puts $f_{ba}(\sqrt{-t}) = 1$, $\mathbf{R} = \mathbf{r}_0$, and $i = 0$. Inserting Eq. (5) into Eq. (2), we find for the transition amplitude

$$T_{\beta\alpha}^{\rm DW} = \langle\Phi_B \mid \hat{\rho} \mid \Phi_A\rangle, \quad (6)$$

where $\hat{\rho}$ is the hadronic transition operator defined as

$$\hat{\rho} = \sum_{j=1,A}(\phi_{s_b m_b \nu_b} \mid \sum_{i=1,a} f_{ba}(\sqrt{-t})t_{ij}(\omega, \mathbf{q}\,) \times X_{\rm DW}(\mathbf{k}_a, \mathbf{k}_b, \mathbf{r}_j) \mid \phi_{s_a m_a \nu_a}), \quad (7)$$

with

$$X_{\rm DW}(\mathbf{k}_a, \mathbf{k}_b, \mathbf{r}) = \chi_b^{(-)^*}(\mathbf{k}_b, \mathbf{r})\chi_a^{(+)}(\mathbf{k}_a, \mathbf{r}). \quad (8)$$

It is clear that $X_{\rm DW}$ describes the projectile distortion effects in the reaction. In the plane wave (PW) approximation, the distorted waves $\chi_a^{(+)}$ and $\chi_b^{(-)^*}$ are replaced by plane waves and $X_{\rm DW}$ is reduced to $X_{\rm DW}(\mathbf{r}) = \exp(i\mathbf{q}\cdot\mathbf{r})$. Although unjustifiable quantitatively, the PW approximation is often useful in the understanding of the more complicated results from the distorted-wave calculations.

B. The effective projectile – target-nucleon interaction

For the evaluation of Eq. (7) we need the explicit representation of $t_{ij}(\omega, \mathbf{q})$. For NN^{-1} excitations the spin-isospin-dependent part of $t_{NN,NN}$ in the NN c.m. frame is given by [37,38]

$$t_{NN,NN}(s,t) = [\alpha - i\gamma\{\boldsymbol{\sigma}_i \cdot \hat{\mathbf{n}} + \boldsymbol{\sigma}_j \cdot \hat{\mathbf{n}}\} + \beta\boldsymbol{\sigma}_i \cdot \hat{\mathbf{n}}\boldsymbol{\sigma}_j \cdot \hat{\mathbf{n}} + \delta\boldsymbol{\sigma}_i \cdot \hat{\mathbf{q}}\boldsymbol{\sigma}_j \cdot \hat{\mathbf{q}} + \epsilon\boldsymbol{\sigma}_i \cdot \hat{\mathbf{p}}\boldsymbol{\sigma}_j \cdot \hat{\mathbf{p}}]\boldsymbol{\tau}_i \cdot \boldsymbol{\tau}_j, \quad (9)$$

where the unit vectors $[\hat{\mathbf{p}}, \hat{\mathbf{n}}, \hat{\mathbf{q}}]$ form a right-handed coordinate system in the two-nucleon center-of-mass frame. They are connected to the initial and final nucleon momenta $\boldsymbol{\kappa}$ and $\boldsymbol{\kappa}'$ by $\mathbf{p} = \boldsymbol{\kappa} + \boldsymbol{\kappa}'$, $\mathbf{q} = \boldsymbol{\kappa} - \boldsymbol{\kappa}'$, and $\hat{\mathbf{n}} = \hat{\mathbf{q}} \times \hat{\mathbf{p}}$. Three different types of spin excitations are possible, namely, a longitudinal one with the spin transfer along the momentum transfer direction $\hat{\mathbf{q}}$ (term δ), and two transverse ones with the spin transfer occurring either in the scattering plane (term ϵ) or perpendicular to the scattering plane (term β). The coefficients α, γ, β, δ, and ϵ are functions of the Mandelstam variables s and t and are determined from NN scattering data.

For ΔN^{-1} excitations the $t_{NN,N\Delta}$ transition operator consists in principle of 16 linearly independent terms [39]. In the present study, however, we assume the following simple form,

$$t_{NN,N\Delta}(s,t) = t'_{N\Delta} J_{\pi N\Delta} \left(\frac{\Lambda'^2_\pi - m_\pi^2}{\Lambda'^2_\pi - t} \right)^2 [(\hat{\boldsymbol{\sigma}}_i \cdot \hat{\mathbf{q}})(\mathbf{S}_j^\dagger \cdot \hat{\mathbf{q}}) + (\boldsymbol{\sigma}_i \times \hat{\mathbf{q}}) \cdot (\mathbf{S}_j^\dagger \times \hat{\mathbf{q}})] \boldsymbol{\tau}_i \cdot \mathbf{T}_j^\dagger, \quad (10)$$

where $J_{\pi N\Delta} = f_{\pi NN} f_{\pi N\Delta} / m_\pi^2 = 800$ MeV fm^3 obtained with the widely accepted values of $f^2_{\pi NN}/4\pi$=0.08 and $f_{\pi N\Delta} = 2 f_{\pi NN}$. The strength parameter $t'_{N\Delta}$ and the cutoff mass Λ'_π in the vertex form factor $[(\Lambda'^2_\pi - m_\pi^2)/(\Lambda'^2_\pi - t)]^2$ are adjusted to experimental data as will be discussed in Sec. III A. The assumed operator is essentially of δ-function type; the only momentum dependence comes from the vertex form factor.

Using the identity $(\boldsymbol{\sigma}_i \times \hat{\mathbf{q}}) \cdot (\mathbf{S}_j^\dagger \times \hat{\mathbf{q}}) = \boldsymbol{\sigma}_i \cdot \hat{\mathbf{n}} \mathbf{S}_j^\dagger \cdot \hat{\mathbf{n}} + \boldsymbol{\sigma}_i \cdot \hat{\mathbf{p}} \mathbf{S}_j^\dagger \cdot \hat{\mathbf{p}}$, we can rewrite Eq. (10) in the form

$$t_{NN,N\Delta}(s,t) = [\beta' \boldsymbol{\sigma}_i \cdot \hat{\mathbf{n}} \mathbf{S}_j^\dagger \cdot \hat{\mathbf{n}} + \delta' \boldsymbol{\sigma}_i \cdot \hat{\mathbf{q}} \mathbf{S}_j^\dagger \cdot \hat{\mathbf{q}} + \epsilon' \boldsymbol{\sigma}_i \cdot \hat{\mathbf{p}} \mathbf{S}_j^\dagger \cdot \hat{\mathbf{p}}] \boldsymbol{\tau}_i \cdot \mathbf{T}_j^\dagger \quad (11)$$

with $\beta' = \delta' = \epsilon' = t'_{N\Delta} J_{\pi N\Delta} [(\Lambda'^2_\pi - m_\pi^2)/(\Lambda'^2_\pi - t)]^2$. The interaction of Eq. (10) or (11) has a very simple spin structure; the strength of the spin-LO term is equal to that of the spin-TR terms. In spite of its simplicity, the assumed t_{ij} can reproduce not only the cross sections but also the spin observables from the reactions with the proton target. (See the discussion in Sec. III A.)

C. Alternative form of the singles cross section

The operator $\hat{\rho}$ defined by Eq. (7) serves as an external field acting on the target nucleus. It is often referred to as the hadronic transition operator. The operator $\hat{\rho}$ depends on the coordinates of the target nucleons only; the projectile coordinates are all integrated over. Note that in distinction from the usual calculation of the DWIA transition amplitude, as in Eq. (2), we have interchanged in Eq. (6) the order of the integrations over the projectile coordinate $\mathbf{R}$ and the target-nucleon coordinate $\mathbf{r}_j$. This has been done since we want to transform the cross section formula into the nuclear response function form by carrying out the sum over the final state $\mid \Phi_B \rangle$. This sum can be performed by inserting Eq. (6) into Eq. (1) and by using the relation

$$\sum_B \delta(\omega - \epsilon_B) \mid \Phi_B \rangle \langle \Phi_B \mid = -\frac{1}{\pi} \mathrm{Im} \left[\frac{1}{\omega - H + i\epsilon} \right], \quad (12)$$

where H is the total Hamiltonian of the residual nuclear system with $H \mid \Phi_B \rangle = \epsilon_B \mid \Phi_B \rangle$. ϵ_B is the excitation energy of nucleus B measured relative to the ground state energy E_A of the target, which we choose as $E_A = 0$. The double differential cross section is then given as

$$\frac{d^2\sigma}{dE_b d\Omega_b} = \frac{E_A E_a E_B E_b}{2\pi^2 \sqrt{\lambda(s, M_a^2, M_A^2)}} \times \frac{p_b}{E_B} \frac{M_a}{E_a} \frac{M_b}{E_b} \frac{1}{2s_a + 1} \sum_{m_a m_b} S, \quad (13)$$

where S is the strength function defined by

$$S = \mathrm{Im}[-\langle \rho \mid G \mid \rho \rangle / \pi], \quad (14)$$

with

$$\mid \rho \rangle \equiv \hat{\rho} \mid \Phi_A \rangle \quad (15)$$

and

$$G = \frac{1}{\omega - H + i\epsilon}. \quad (16)$$

$\mid \rho \rangle$ of Eq. (15) is the doorway state excited initially by the external operator $\hat{\rho}$; G propagates this state resulting in the so called continuum wave function

$$\mid \Psi \rangle = G \mid \rho \rangle. \quad (17)$$

With the aid of $\mid \Psi \rangle$ we can express S of Eq. (14) in an alternative form as

$$S = \Im[-\langle \rho \mid \Psi \rangle / \pi]. \quad (18)$$

Equation (13) together with (18) provides the final cross section formula expressed in terms of $\mid \Psi \rangle$ of Eq. (17). Now it is our task to calculate $\mid \Psi \rangle$.

D. The correlated source function method

The correlated source function method provides a very efficient way of calculating $\mid \Psi \rangle$. The method makes use of the fact that the Hamiltonian H of the target system is given by

$$H = H_0 + V_{\mathrm{ph}}, \quad (19)$$

where H_0 is the single-particle Hamiltonian and V_{ph} is the residual ph interaction. In the following we assume that the target is a double magic nucleus with spin parity $I_A^\pi = 0^+$. Furthermore, we approximate the target ground state wave function by a single Slater determinant of the independent-particle model. This means that we choose $\mid \Phi_A \rangle$ to be an eigenfunction of H_0 instead of H, i.e.,

$$H_0 \mid \Phi_A\rangle = E_A \mid \Phi_A\rangle \qquad (E_A = 0). \tag{20}$$

The above approximation neglects the effects of $V_{\rm ph}$ on the ground state wave function. The effects of $V_{\rm ph}$ are included, however, in the wave function of the excited states. This different treatment of $V_{\rm ph}$ for the ground state and the excited states is known as the Tamm-Dancoff approximation. To proceed we split H_0 into $H_0 = H_C + H_p$, where H_C is the Hamiltonian of the hole nucleus C and H_p is the Hamiltonian of the excited particle p. The spectrum of H_C is defined by

$$H_C \mid \Phi_h\rangle = E_h \mid \Phi_h\rangle, \tag{21}$$

where E_h is the hole energy. Finally, the Hamiltonian of the excited particle p is given by

$$H_p = T_p + U_p + i\frac{\Gamma_p(s_\Delta)}{2} \quad (p = \Delta \text{ or } N), \tag{22}$$

where T_p is the kinetic energy operator, $U_p = V_p + iW_p$ is a complex one-body potential, and $\Gamma_{p=\Delta}$ is the free decay width of the Δ ($\Gamma_{p=N} = 0$, of course). Note that $\Gamma_\Delta(s_\Delta)$ is a function of the intrinsic energy of the Δ, and is related to the energy transfer ω by $s_\Delta = \omega - H_\Delta - E_h$. We follow Ref. [27] in dealing with the H_Δ dependence of $\Gamma_\Delta(s_\Delta)$.

Using the Hamiltonian of Eq. (19), we can derive the following integral equation for the continuum wave function:

$$\mid \Psi\rangle = G_0 \mid \rho\rangle + G_0 V_{\rm ph} \mid \Psi\rangle, \tag{23}$$

where G_0 is the unperturbed Green's function defined by

$$G_0 = \frac{1}{\omega - H_0 + i\epsilon}. \tag{24}$$

To solve Eq. (23) we first transform the integral equation into an equivalent integral equation [40]

$$\mid \Lambda\rangle = \mid \rho\rangle + V_{\rm ph} G_0 \mid \Lambda\rangle, \tag{25}$$

so that

$$\mid \Psi\rangle \equiv G_0 \mid \Lambda\rangle. \tag{26}$$

Note that $\mid \Lambda\rangle$ thus defined plays in Eq. (26) a similar role as $\mid \rho\rangle$ in Eq. (17). We call $\mid \Lambda\rangle$ the correlated source function since it includes the correlations due to $V_{\rm ph}$.

Equation (25) is now solved by first integrating over all coordinates, except the radial coordinate of particle p. In this way the equation is reduced to a set of coupled-channel (CC) equations for the radial wave functions of particle p. In order to achieve this we expand both $\mid \Lambda\rangle$ and $\mid \rho\rangle$ in terms of the channel wave functions

$$\mid [y_p \Phi_h]_{jm}\rangle = \sum_{m_p m_h} \langle j_p m_p j_h m_h | jm\rangle \mid y_{j_p m_p} \Phi_{j_h m_h}\rangle, \tag{27}$$

where $y_{j_p m_p}$ is the spin-angle wave function of p and $\Phi_{j_h m_h}$ is the hole-nucleus wave function of Eq. (21). The channel expansion is then given by

$$\begin{aligned}
\mid \Lambda\rangle = & \sum_{j_t \ell_t m_{j_t} m_{\ell_t} m_{s_t}} \sqrt{2}\langle s_b m_b s_a - m_a \mid s_t m_{s_t}\rangle (-1)^{\ell_t + m_{\ell_t}} \\
& \times \langle j_t m_{j_t} s_t - m_{s_t} \mid \ell_t - m_{\ell_t}\rangle \sum_{\rm ph}^{N_c} \frac{\lambda_{\rm ph}(r)}{r} \mid [y_p \Phi_h]_{j_t m_{j_t}}\rangle, \\
\mid \rho\rangle = & \sum_{j_t \ell_t m_{j_t} m_{\ell_t} m_{s_t}} \sqrt{2}\langle s_b m_b s_a - m_a \mid s_t m_{s_t}\rangle (-1)^{\ell_t + m_{\ell_t}} \\
& \times \langle j_t m_{j_t} s_t - m_{s_t} \mid \ell_t - m_{\ell_t}\rangle \sum_{\rm ph}^{N_c} \frac{\rho_{\rm ph}(r)}{r} \mid [y_p \Phi_h]_{j_t m_{j_t}}\rangle,
\end{aligned} \tag{28}$$

where j_t, ℓ_t, and s_t are the total, orbital, and spin angular momenta transferred in the reaction, respectively; m_{j_t}, m_{ℓ_t}, and m_{s_t} are the corresponding angular momentum projections. The quantities $\lambda_{\rm ph}(r)$ and $\rho_{\rm ph}(r)$ are the correlated and uncorrelated radial source functions, respectively. Note that both radial source functions depend on the quantum numbers $j_t \ell_t m_{\ell_t}$, though these indices are not shown explicitly. The sum involved in Eq. (28) is taken over all ph pairs. The total number of ph pairs is denoted by N_c.

Inserting the expansions of Eq. (28) into Eq. (25), we obtain a set of CC equations for $\lambda_{\rm ph}(r)$,

$$\begin{aligned}
\lambda_{\rm ph}(r) = \rho_{\rm ph}(r) + \sum_{p'h'} \int dr' dr'' V^{j_t}_{{\rm ph},p'h'}(r, r') \\
\times g^{(+)}_{p'h'}(r', r'') \lambda_{p'h'}(r''),
\end{aligned} \tag{29}$$

where the ph matrix elements $V^{j_t}_{{\rm ph},p'h'}(r, r')$ are defined by

$$V^{j_t}_{{\rm ph},p'h'}(r, r') = rr'([y_{p'} \Phi_{h'}]_{j_t} | V_{\rm ph} | [y_p \Phi_h]_{j_t}). \tag{30}$$

Here the parentheses denote an integration over the channel variables. Introducing column vectors of dimension $1 \times N_c$

$$\mid \lambda\rangle = \begin{pmatrix} \lambda_{p_1 h_1} \\ \cdots \\ \cdots \end{pmatrix}, \tag{31}$$

$$\mid \rho\rangle = \begin{pmatrix} \rho_{p_1 h_1} \\ \cdots \\ \cdots \end{pmatrix}, \tag{32}$$

we can write the CC equations in matrix form as

$$| \lambda\rangle = | \rho\rangle + \mathcal{V}\mathcal{G}_0 | \lambda\rangle, \tag{33}$$

where $\mathcal{V}$ is the interaction matrix

$$(\mathcal{V})_{\mathrm{ph},p'h'}(r,r') = V^{j_t}_{\mathrm{ph},p'h'}(r,r') \tag{34}$$

of dimension $N_c \times N_c$ and $\mathcal{G}_0$ is the diagonal Green's function matrix defined by

$$(\mathcal{G}_0)_{\mathrm{ph},p'h'} = g^{(+)}_{\mathrm{ph}}\delta_{\mathrm{ph},p'h'}. \tag{35}$$

In the last equation $g^{(+)}_{\mathrm{ph}}$ is the radial optical model Green's function. Note that the operation of $\mathcal{G}_0$ (and $\mathcal{V}$) onto $| \lambda\rangle$ in Eq. (33) involves a radial integration besides the matrix multiplication.

Equation (33) is the final equation to be solved. The source functions $\rho_{\mathrm{ph}}(r)$ can be calculated in a straightforward manner. The details of the calculation are presented in Appendix A, along with the results for $V^{j_t}_{\mathrm{ph},p'h'}(r,r')$. The merit of solving $| \lambda\rangle$ first instead of the corresponding $| \psi\rangle$, defined below by Eq. (37), lies in the fact that $\lambda_{\mathrm{ph}}(r)$ is a localized (bound) function. This is so since $\rho_{\mathrm{ph}}(r)$ is proportional to the radial hole wave function $u_h(r)$. Similarly, the interaction terms $V^{j_t}_{\mathrm{ph},p'h'}(r,r')$ are also localized because they include $u_h(r)$, too [see Eq. (A15)]. This fact makes it possible to expand $| \lambda\rangle$ in terms of a set of orthonormal basis functions. The problem can then be reduced to solving a set of inhomogeneous linear equations for the expansion coefficients (Lanczos method). These equations are derived by inserting the expansion into the original integral equation (25). It turns out that this method enables us to solve Eq. (33) in a very efficient way. The Lanczos method we used in solving these equations is described in Appendix B.

Once $| \lambda\rangle$ is known, it is easy to calculate $| \Psi\rangle$. In partial wave expansion $| \Psi\rangle$ is given by

$$| \Psi\rangle = \sum_{j_t \ell_t m_{j_t} m_{\ell_t} m_{s_t}} \sqrt{2}\langle s_b m_b s_a - m_a \mid s_t m_{s_t}\rangle(-1)^{\ell_t + m_{\ell_t}} \times \langle j_t m_{j_t} s_t - m_{s_t} \mid \ell_t - m_{\ell_t}\rangle \sum_{\mathrm{ph}}^{N_c} \frac{\psi_{\mathrm{ph}}(r)}{r} \mid [y_p \Phi_h]_{j_t m_{j_t}}\rangle. \tag{36}$$

It is easy to see that the column vector $| \psi\rangle$ defined by

$$| \psi\rangle = \begin{pmatrix} \psi_{\mathrm{ph}} \\ \cdots \\ \cdots \end{pmatrix} \tag{37}$$

can be given as

$$| \psi\rangle = \mathcal{G}_0 | \Lambda\rangle. \tag{38}$$

E. The residual ph interaction

The residual ph interaction V_{ph} is treated within the $(\pi + \rho + g'_0)$ model (see [7] and references therein). In the ρ exchange we keep only the tensor interaction and drop the central part assuming that the latter can be effectively included in the short-range interaction. The matrix elements $V^{j_t}_{\mathrm{ph},p'h'}$ consist then of the four couplings $V_{NN^{-1},NN^{-1}}$, $V_{NN^{-1},\Delta N^{-1}}$, $V_{\Delta N^{-1},NN^{-1}}$, and $V_{\Delta N^{-1},\Delta N^{-1}}$. We write V_{ph} in terms of spin-LO and spin-TR components according to

$$V_{\mathrm{ph}}(\omega,q) = \left[V^{(\mathrm{LO})}_{\mathrm{ph}}(\omega,q)\mathcal{S}_p \cdot \mathbf{q}\, \mathcal{S}^\dagger_{p'} \cdot \mathbf{q} + V^{(\mathrm{TR})}_{\mathrm{ph}}(\omega,q)(\mathcal{S}_p \times \mathbf{q}) \cdot (\mathcal{S}^\dagger_{p'} \times \mathbf{q})\right] \mathcal{T}_p \cdot \mathcal{T}^\dagger_{p'}, \tag{39}$$

where

$$V^{(\mathrm{LO})}_{\mathrm{ph}}(\omega,q) = J_\pi(\omega,q)\frac{f_{\pi Np} f_{\pi Np'}}{f^2_{\pi NN}}\left[g'_{pp'} + \frac{q^2}{\omega^2 - q^2 - m^2_\pi + i\epsilon} - \frac{2}{3}\frac{J_\rho(\omega,q)}{J_\pi(\omega,q)}\frac{q^2}{\omega^2 - q^2 - m^2_\rho + i\epsilon}\right] \tag{40}$$

and

$$V^{(\mathrm{TR})}_{\mathrm{ph}}(\omega,q) = J_\pi(\omega,q)\frac{f_{\pi Np} f_{\pi Np'}}{f^2_{\pi NN}}\left[g'_{pp'} + \frac{1}{3}\frac{J_\rho(\omega,q)}{J_\pi(\omega,q)}\frac{q^2}{\omega^2 - q^2 - m^2_\rho + i\epsilon}\right]. \tag{41}$$

In Eq. (39) $\mathcal{S}_p$ is the spin (transition) operator with $\mathcal{S}_p \equiv \boldsymbol{\sigma}$ (**S**) for $p = N$ (Δ). Similarly, $\mathcal{T}_p$ is the isospin (transition) operator with $\mathcal{T}_p \equiv \boldsymbol{\tau}$ (**T**) for $p = N$ (Δ). The force strength parameters J_π and J_ρ are defined by

$$J_\pi(\omega,q) = \frac{f^2_{\pi NN}}{m^2_\pi}\left(\frac{\Lambda^2_\pi - m^2_\pi}{\Lambda^2_\pi - t}\right)^2 \tag{42}$$

and

$$J_\rho(\omega,q) = \frac{f^2_{\rho NN}}{m^2_\rho}\left(\frac{\Lambda^2_\rho - m^2_\rho}{\Lambda^2_\rho - t}\right)^2, \tag{43}$$

respectively, where $f^2_{\rho NN}/4\pi$=4.86 and $f_{\rho N\Delta} = 2f_{\rho NN}$, while the values of $f_{\pi NN}$ and $f_{\pi N\Delta}$ were already given

in Sec. II B.

The quantities in parentheses in Eqs. (42) and (43) are the form factors which describe the finite size of the meson-nucleon vertices. Use is made of the cutoff masses $\Lambda_\pi = 1.2$ GeV and $\Lambda_\rho = 2.0$ GeV. The three Landau-Migdal parameters g'_{NN}, $g'_{N\Delta}$, and $g'_{\Delta\Delta}$ are to be adjusted to reproduce the experimental data. The value of g'_{NN} (=0.6) has been determined from the excitation energy of the giant Gamow-Teller resonance (see [7] and references therein). The value of $g'_{N\Delta}$ is less well known and only has some constraints from Brueckner G-matrix calculations (see [7] and references therein). Further, the value of $g'_{\Delta\Delta}$ is not known. In the present study, we treat both $g'_{N\Delta}$ and $g'_{\Delta\Delta}$ as free parameters which have to be determined from the fit of the calculated spectra to the experimental data.

F. The decomposition of the inclusive cross section into components

The inclusive cross section of Eq. (13) can be decomposed into partial cross sections corresponding to different physical processes. These processes are schematically represented by the graphs in Figs. 3(a)–(e). Only the lowest-order diagrams are shown. We distinguish between coherent pion production (a), quasifree decay (b), nucleon knockout (c), Δ spreading (d), and nucleon spreading (e). The incoherent sum of these various processes gives the inclusive, single-step cross section.

The first step of the decomposition of the cross section is to rewrite S in terms of $|\Lambda\rangle$. Inserting Eq. (25) into Eq. (18) we obtain

$$S = \frac{1}{\pi}\mathrm{Im}\{\langle\Psi \mid V^\dagger_{\rm ph} \mid \Psi\rangle - \langle\Lambda \mid G_0 \mid \Lambda\rangle\}. \tag{44}$$

Using now the identity

$$\mathrm{Im}G_0 = -\pi\Omega^{(-)}\delta(E - H_C - T_p)\Omega^{(-)\dagger} + G_0^\dagger(W_N + W_\Delta - \Gamma_\Delta/2)G_0, \tag{45}$$

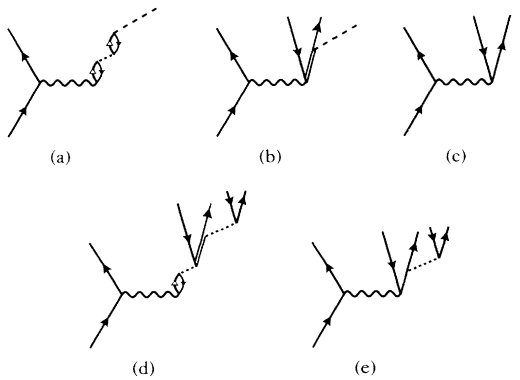

FIG. 3. Schematic representation of the physical processes included in the analysis of the data. For each process only the lowest-order approximation is shown. The diagrams have the following meaning: (a) coherent pion production, (b) quasifree Δ decay, (c) nucleon knockout, (d) Δ spreading, (e) nucleon spreading.

where $\Omega^{(-)} = 1 + (U_p + \frac{i}{2}\Gamma_\Delta)G_0$ is the Moeller wave operator and W_N is the imaginary part of the optical potential of the nucleon particle $p = N$, we obtain the following decomposition of the strength function S of Eq. (44):

$$S = S_{\rm CPP} + S_{\rm QF} + S_{\rm SP} + S_{\rm KO} + S_{\rm KF}. \tag{46}$$

Here the partial strength functions are defined by

$$S_{\rm CPP} = \frac{1}{\pi}\langle\Psi \mid \mathrm{Im}V^\dagger_{\rm ph} \mid \Psi\rangle, \tag{47}$$

$$S_{\rm QF} = \frac{1}{\pi}\langle\Psi \mid \Gamma_\Delta/2 \mid \Psi\rangle, \tag{48}$$

$$S_{\rm SP} = \frac{1}{\pi}\langle\Psi \mid -W_\Delta \mid \Psi\rangle, \tag{49}$$

$$S_{\rm KO} = \mathrm{Im}\langle\Psi \mid \Omega^{(-)}\delta(E - H_C - T_p)\Omega^{(-)\dagger} \mid \Psi\rangle, \tag{50}$$

$$S_{\rm KF} = \frac{1}{\pi}\langle\Psi \mid -W_N \mid \Psi\rangle. \tag{51}$$

The physical significance of the various components is as follows. $S_{\rm CPP}$ describes the strength function of the coherent pion production (CPP) process $A+a \to b+A+\pi$, where the residual nucleus is left in its ground state [see Fig. 3(a)]. This strength function is proportional to $\mathrm{Im}V^\dagger_{\rm ph}$. $\mathrm{Im}V^\dagger_{\rm ph}$ comes from the pion pole in the π-exchange interaction of Eq. (40). $S_{\rm QF}$ describes the strength function of the quasifree (QF) decay process where the Δ excitation in the nucleus is followed by the decay $\Delta \to \pi+N$ [see Fig. 3(b)]. $S_{\rm SP}$ denotes the spreading (SP) strength function that results from Δ conversion processes, such as $\Delta + N \to N + N$ [Fig. 3(d)]. $S_{\rm KO}$ is the strength function for the nucleon knockout (KO) process [Fig. 3(c)], and finally $S_{\rm KF}$ is the strength function for the nucleon knockout-fusion (KF) process where the excited nucleon knocks out additional nucleons from the target [Fig. 3(e)]. Among these five strength functions, $S_{\rm QF}$, $S_{\rm SP}$, and $S_{\rm KF}$ can be calculated in a straightforward manner from Eqs. (48), (49), and (51). This is not the case, however, for $S_{\rm KO}$ and $S_{\rm CCP}$. They are more easily calculated from the alternative expressions

$$S_{\rm KO} = \frac{1}{\pi}\{-\langle\Lambda \mid G_0 \mid \Lambda\rangle\} - S_{\rm KF} - S_{\rm SP} - S_{\rm QF}, \tag{52}$$

$$S_{\rm CPP} = S - \frac{1}{\pi}\{-\langle\Lambda \mid G_0 \mid \Lambda\rangle\}. \tag{53}$$

In terms of the partial strength functions S_α (α=CPP, QF, SP, KO, KF) the double differential, partial cross sections are given by

$$\frac{d^2\sigma_\alpha}{dE_b d\Omega_b} = \frac{E_A E_a E_B E_b}{2\pi^2\sqrt{\lambda(s, M_a^2, M_A^2)}}\frac{p_b}{E_B}\frac{M_a}{E_a}\frac{M_b}{E_b}\sum_{m_a m_b} S_\alpha. \tag{54}$$

G. Exclusive cross section for coherent pion production

The most interesting component of the partial cross sections of Eq. (54) derived in the previous section is that

of the coherent pion decay (α=CPP). In the CPP process, the excited nucleus deexcites to the target ground state $\mid \Phi_A\rangle$ by emission of a pion of energy $E_\pi = \omega_L - E_R$, where E_R is the recoil energy of the final nucleus A. The cross section given by Eq. (54) with $\alpha = CPP$, however, involves an integral over the angle of the emitted pion. In what follows, we derive the differential cross section starting from Eq. (54) with $S_{\rm CPP}$ given by Eq. (47). For this purpose, we first notice that in the Δ resonance region $\mathrm{Im}V^\dagger_{\rm ph}$ comes exclusively from the π-exchange interaction. Therefore $\mathrm{Im}V^\dagger_{\rm ph}$ can be written as

$$\frac{1}{\pi}\mathrm{Im}V^\dagger_{\rm ph} = V^\dagger_{\Delta N\pi} \mid \Phi_A\rangle\delta(\omega - T_\pi)\langle\Phi_A \mid V_{\Delta N\pi}$$
$$= \int \frac{d^3\mathbf{p}_\pi}{(2\pi)^3 2E_\pi} V^\dagger_{\Delta N\pi} \mid \Phi_A\phi(\mathbf{p}_\pi)\rangle$$
$$\times\delta(\omega - E_\pi)\langle\Phi_A\phi(\mathbf{p}_\pi) \mid V_{\Delta N\pi}, \qquad (55)$$

where T_π is the kinetic energy operator of the pion; $V_{\Delta N\pi}$ is the $\pi N\Delta$ interaction Hamiltonian

$$V_{\Delta N\pi} = \frac{f_{\pi N\Delta}}{m_\pi}\mathbf{S}^\dagger\cdot\boldsymbol{\kappa}_\pi F(\kappa_\pi^2)T^\dagger_\mu \qquad (56)$$

expressed in terms of the variables of the Δ rest frame (involving the relative pion-nucleon momentum $\boldsymbol{\kappa}_\pi$). Inserting Eq. (55) into (47) and the result of that into (54), we find that the CPP cross section can be expressed as

$$\frac{d^2\sigma_{\rm CPP}}{dE_b d\Omega_b} = \int d\Omega_\pi \frac{d^3\sigma_{\rm CPP}}{dE_b d\Omega_b d\Omega_\pi}, \qquad (57)$$

where

$$\frac{d^3\sigma_{\rm CPP}}{dE_b d\Omega_b d\Omega_\pi} = \frac{E_A E_a E_B E_b}{(2\pi)^5\sqrt{\lambda(s, M_a^2, M_A^2)}}\frac{p_b p_\pi}{E_B}\frac{M_a}{E_a}\frac{M_b}{E_b}$$
$$\times\overline{\sum} \mid \langle\Phi_A\phi(\mathbf{p}_\pi) \mid V^\dagger_{\Delta N\pi} \mid \Psi\rangle \mid^2 \qquad (58)$$

is the triple differential exclusive cross section.

In order to calculate the transition matrix elements in Eq. (58), we use the partial wave expansion Eq. (36) for $\mid \Psi\rangle$ and also the partial wave expansion of $\mid \phi(\mathbf{p}_\pi)\rangle$. After some lengthy algebra we obtain

$$\langle\Phi_A\phi(\mathbf{p}_\pi) \mid V^\dagger_{\Delta N\pi} \mid \Psi\rangle = \sum_{j_t\ell_t m_{j_t} m_{\ell_t}} \langle s_b m_b s_a - m_a \mid s_t m_{s_t}\rangle$$
$$\times(-1)^{\ell_t m_{\ell_t}}\langle j_t m_{j_t} s_t - m_{s_t} \mid \ell_t m_{\ell_t}\rangle\beta_{j_t\ell_t m_{\ell_t}}, \qquad (59)$$

where

$$\beta_{j_t\ell_t m_{\ell_t}} = F(\kappa_\pi^2)2\sqrt{4\pi}\sum_{\substack{\ell_t j_t m_j, l_\pi \\ l_h l_\Delta j_h j_\Delta}} (-1)^{j_t - m_{j_t}} Y^{m_{j_t}}_{j_t}(\hat{k}_\pi)$$
$$\times i^{l_\Delta + l_h - l_\pi}\hat{j}_\Delta\hat{j}_h\hat{l}_h\hat{l}_\pi\,(l_h 0 l_\pi 0 \mid l_\Delta 0)\,(J010 \mid l_\pi 0)\begin{pmatrix} l_\Delta & \frac{3}{2} & j_\Delta \\ l_h & \frac{1}{2} & j_h \\ l_\pi & 1 & j_t \end{pmatrix}$$
$$\times\int dr\psi^{j_t\ell_t m_{\ell_t}}_{\rm ph}(r) j_{l_\pi}(p_\pi r) u_h(r)\times ISO \qquad (60)$$

is the reduced transition amplitude. In the last equation ISO is the isospin factor which amounts to ISO= $1(1/\sqrt{3})$ for the $\Delta^{++}\to p+\pi^+$ ($\Delta^+\to n+\pi^+$) transition. Insertion of (59) into (58) results in the triple differential cross section in the form

$$\frac{d^3\sigma_{\rm CPP}}{dE_b d\Omega_b d\Omega_\pi} = \frac{E_A E_a E_B E_b}{(2\pi)^5\sqrt{\lambda(s, M_a^2, M_A^2)}}\frac{p_b p_\pi}{E_B}\frac{M_a}{E_a}\frac{M_b}{E_b}\frac{1}{(2s_a+1)(2I_A+1)}$$
$$\times\left|\sum_{j_t\ell_t m_{j_t} m_{\ell_t}} (-1)^{\ell_t m_{\ell_t}}\langle j_t m_{j_t} s_t - m_{s_t} \mid \ell_t m_{\ell_t}\rangle\beta_{j_t\ell_t m_{\ell_t}}\right|^2, \qquad (61)$$

where I_A is the spin of the target ground state. From this cross section formula we can calculate the angular distributions for the coherent pion decay [23]. We remark that similar exclusive cross section formulas can also be derived for the other partial cross sections, such as for α=QF, SP, etc. These cross section formulas will be published elsewhere [41].

H. Spin observables

Another important source of information on the spin structure of the $t_{NN,N\Delta}$ transition amplitude as well as the π correlations in the nucleus is provided by the measurement of the spin observables. In particular, the projectile polarization-transfer observables are sensitive to the spin-LO and spin-TR response functions. The polarization-transfer observables can be expressed in terms of the Cartesian polarization-transfer coefficients [42,43]

$$D_{mm'}(\mathbf{k}_i, \mathbf{k}_f) = \frac{\mathrm{Tr}(\rho^\dagger\sigma_m\psi\sigma_{m'})}{\mathrm{Tr}(\rho^\dagger\psi)},$$
$$m = x, y, z;\ m' = x', y' z', \qquad (62)$$

where the σ_m ($m = x, y, z$) are the Pauli spin matrices acting on the projectile system. We choose the z axis (z' axis) along the beam direction $\mathbf{k}_a$ ($\mathbf{k}_b$) and the y axis perpendicular to the scattering plane parallel to $\hat{\mathbf{n}} = (\mathbf{k}_a \times \mathbf{k}_b)/ \mid \mathbf{k}_a \times \mathbf{k}_b \mid$. The x axis is then chosen so as to obtain a right-handed coordinate frame, i.e., $\hat{\mathbf{x}} = \hat{\mathbf{y}} \times \hat{\mathbf{z}}$ ($\hat{\mathbf{x}}' = \hat{\mathbf{y}}' \times \hat{\mathbf{z}}'$). Note that the coordinate frames in the incident and exit channels are related through a rotation around the y axis by the scattering angle θ. The primed index on $D_{mm'}$ reminds us that the initial and final states of the beam polarization do not need to be referred to the same coordinate frame.

For the discussion of the spin observables it is useful to define the spin-LO and spin-TR strength functions $S_{\rm LO}$ and $S_{\rm TR}$. They are defined by

$$S_i = \mathrm{Im}[-\langle \rho_i | G | \rho_i \rangle / \pi] \qquad (i = \mathrm{LO\ or\ TR}), \tag{63}$$

where

$$|\rho_i\rangle = \hat{\mathbf{O}}_i |\Phi_A\rangle, \tag{64}$$

with

$$\hat{\mathbf{O}}_{\rm LO} = e^{i\mathbf{q}\cdot\mathbf{r}} (\mathbf{S} \cdot \hat{\mathbf{q}}) \hat{\mathbf{T}}_-, \tag{65}$$

and

$$\hat{\mathbf{O}}_{\rm TR} = \frac{1}{\sqrt{2}} e^{i\mathbf{q}\cdot\mathbf{r}} (\mathbf{S} \times \hat{\mathbf{q}}) \hat{\mathbf{T}}_-. \tag{66}$$

The factor $1/\sqrt{2}$ in Eq. (66) has been included for convenience because there are two transverse directions, $\hat{\mathbf{n}}$ and $\hat{\mathbf{n}} \times \hat{\mathbf{q}}$, but only one longitudinal direction $\hat{\mathbf{q}}$. In the present paper we shall restrict our analysis of the spin observables to forward scattering ($\theta = 0°$) where the scattering problem has a symmetry around the beam axis. In this case there exist only two interesting polarization transfer coefficients, namely the one with the spin transfer along the beam direction (D_{zz}) and the other with the spin transfer perpendicular to the beam direction (D_{xx}). Assuming that the cross section in the Δ resonance region is dominated by spin-flip processes, D_{zz} and D_{xx} can be expressed as [43]

$$D_{xx}(0°) = \frac{-|S_{\rm LO}|^2}{|S_{\rm LO}|^2 + 2|S_{\rm TR}|^2}, \tag{67}$$

$$D_{zz}(0°) = \frac{|S_{\rm LO}|^2 - 2|S_{\rm TR}|^2}{|S_{\rm LO}|^2 + 2|S_{\rm TR}|^2}. \tag{68}$$

These equations show that the spin transfer coefficients are sensitive to the π correlations through $S_{\rm LO}$.

III. RESULTS AND DISCUSSION

A. The $t_{NN,N\Delta}$ transition operator

The two parameters $t'_{N\Delta}$ and Λ'_π involved in the effective $NN \to N\Delta$ transition operator defined in Eq. (10) are adjusted to the experimental data. In Fig. 4(a) we show the zero-degree spectrum of the basic reaction $p(p,n)\Delta^{++}$ at $E = 800$ MeV incident energy obtained with the interaction of Eq. (10) using $t'_{N\Delta} = 0.55$ and $\Lambda'_\pi = 650$ MeV. Both the shape and the magnitude of the experimental cross section [3] are reproduced very well. From this comparison the parameters $t'_{N\Delta}$ and Λ'_π are fixed. In Fig. 4(b) we show a similar analysis of the $p(^3\mathrm{He},t)\Delta^{++}$ reaction at E=2 GeV and zero degrees. In this case the finite size of the projectile has to be taken into account. Because of the D-state admixture to the ^{3}He and triton $(1s)^3$ wave functions the spin-LO and spin-TR form factors $F_{\rm LO}(t)$ and $F_{\rm TR}(t)$ have a different momentum transfer (t) dependence. Faddeev calculations show [44] that $F_{\rm LO}(t)$ falls off much more slowly than $F_{\rm TR}(t)$ with t. Guided by these calculations we parametrize the form factors as $F_{\rm LO} = e^{\alpha_{\rm LO} t}$ and $F_{\rm TR} = e^{\alpha_{\rm TR} t}$, where $\alpha_{\rm LO} = 0.4$ fm^2 and $\alpha_{\rm TR} = 0.56$ fm^2. A plot of the form factors is shown in Fig. 5. With these form factors and the $t'_{N\Delta}$ and Λ'_π values fixed above we can reproduce the $p(^3\mathrm{He},t)\Delta^{++}$ data rather well, as can be seen from Fig. 4(b).

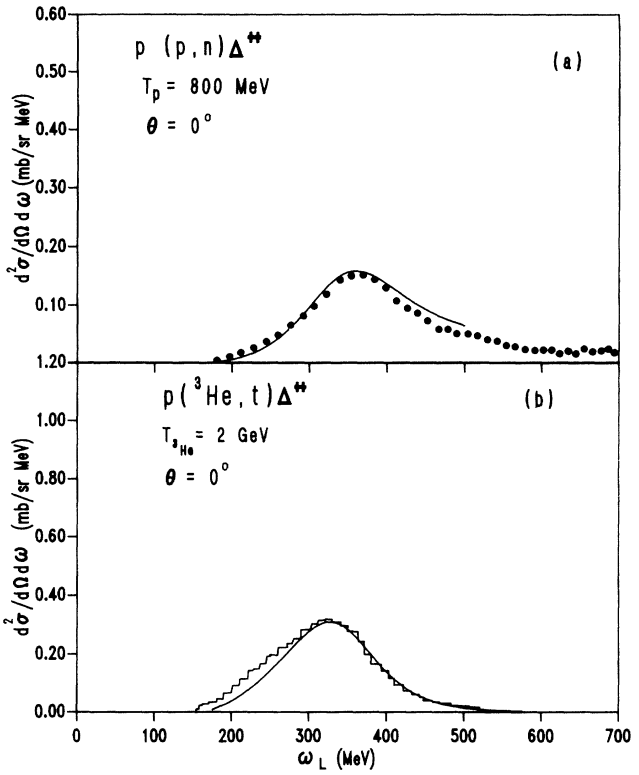

FIG. 4. Zero-degree spectra for charge exchange reactions off the proton target. (a) The $p(p,n)\Delta^{++}$ reaction at E=800 MeV. The data are taken from Ref. [3]. (b) The $p(^3\mathrm{He},t)\Delta^{++}$ reaction at E=2 GeV. The data are taken from Ref. [2].

In order to check the spin structure of the transition amplitude $t_{NN,N\Delta}$, i.e., to find the ratio between the LO and TR interaction components, we analyze the spin observables of the $p(\mathbf{p},\mathbf{n})\Delta^{++}$ spin-flip transfer reaction at $\theta = 0°$. In case of a proton target the polarization transfer coefficients of Eqs. (67) and (68) reduce to

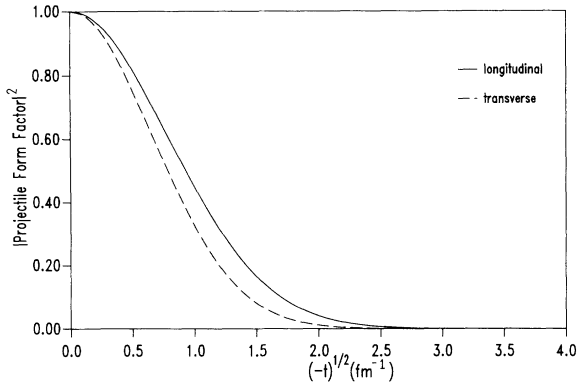

FIG. 5. The spin-longitudinal (solid) and spin-transverse (dashed) form factors squared for the (^{3}He,t) projectile-ejectile system.

$$D_{zz} = \frac{|\delta'|^2 - |\beta'|^2 - |\epsilon'|^2}{|\delta'|^2 + |\beta'|^2 + |\epsilon'|^2}, \tag{69}$$

$$D_{xx} = \frac{-|\delta'|^2}{|\delta'|^2 + |\beta'|^2 + |\epsilon'|^2}, \tag{70}$$

where β', ϵ', and δ' are the interaction components of Eq. (11). In Fig. 6 we show the measured [45] spin transfer coefficients D_{xx} and D_{zz} for the $p(\mathbf{p},\mathbf{n})\Delta^{++}$ reaction at E=800 MeV. Note that the measured values of $D_{zz} = D_{xx} = -1/3$ can only be reproduced by the interaction of Eq. (11) if the force components are all equal, i.e., $|\delta'| = |\beta'| = |\epsilon'|$. This implies that the Δ excitation process is dominantly spin transverse with a cross section ratio of TR/LO= $(|\beta'|^2 + |\epsilon'|^2)/|\delta'|^2$=2/1. We remark that this TR/LO ratio also explains the observed tensor analyzing power data of the $p(\mathbf{d},2p)\Delta^0$ reaction [46]. In addition, the $p(\mathbf{d},2p)\Delta^0$ data require that $t_{NN,N\Delta}$ is nearly constant in the $(\omega,\mathbf{q})$ range relevant to the Δ resonance region [47]. Both conditions are satisfied by $t_{NN,N\Delta}$ of Eq. (10).

B. Analysis of ^{12}C(p,n) and ^{12}C(^{3}He,t) reaction spectra

1. Input parameters

With the formalism described in Sec. II we have calculated energy spectra at various scattering angles for the ^{12}C(p,n) reaction at E=800 MeV and the ^{12}C(^{3}He,t) reaction at E=2 GeV. The calculations were performed by using the optical potential parameters of Table I. For the target ground state wave function a pure shell model configuration was assumed. The single-particle wave functions were generated from a Woods-Saxon potential with the geometrical parameters $a_0 = a_{so}$=0.53 fm, and $r_0 = r_{so} = r_C$=1.20 fm and the spin-orbit strength V_{so} =5.53 MeV. The strength parameters for the proton and neutron potentials were fixed as V_p=65.7 MeV and V_n=66.0 MeV, respectively. The Δ-nucleus optical potential, $U_\Delta = V_\Delta + iW_\Delta$, was taken as a (complex) Woods-Saxon potential with the radius parameter

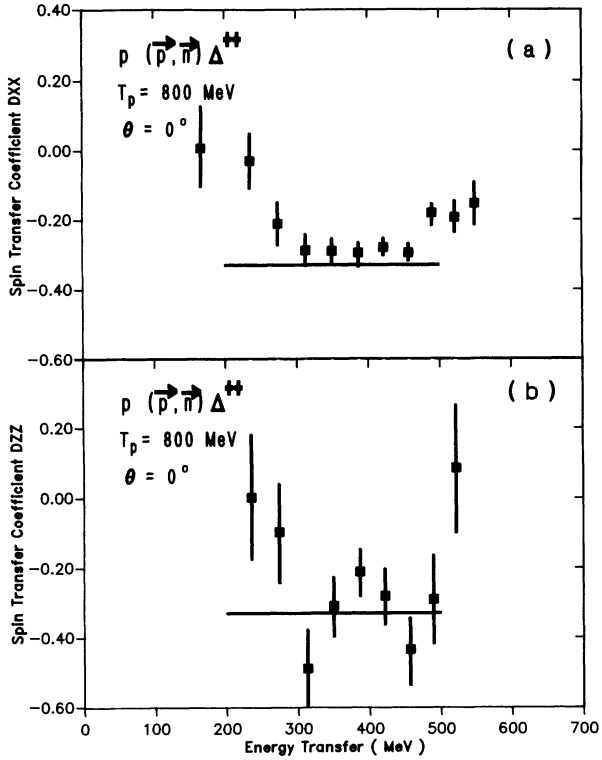

FIG. 6. Calculated spin transfer coefficients for the $p(\mathbf{p},\mathbf{n})\Delta^{++}$ reaction at E=800 MeV in comparison with the experimental data [44].

$R = 1.1A^{\frac{1}{3}}$ fm, diffuseness a=0.53 fm, and the depths $V_\Delta = -35$ MeV and $W_\Delta = -40$ MeV for the real and imaginary potentials, respectively [34]. The real part V_Δ was assumed to be the sum of the Δ-nucleus single-particle potential (depth of −65 MeV) and the Δ spreading potential (strength of +30 MeV); W_Δ was assumed to be energy dependent with the parametrization $W_\Delta(\omega) = -0.24\omega + 7.6$ MeV for $\omega \leq 200$ MeV and $W_\Delta(\omega) = -40$ MeV for $\omega \geq 200$ MeV. The free decay width $\Gamma_\Delta(s_\Delta)$ was parametrized in the usual form [9].

The two unknown Landau-Migdal parameters $g'_{N\Delta}$ and $g'_{\Delta\Delta}$ in V_{ph} were fixed from an overall fit of the calculated cross sections to experiment. The values thus determined are $g'_{N\Delta} = g'_{\Delta\Delta} = 0.333$. The experimental data thus require the minimal value for $g'_{N\Delta}$ and $g'_{\Delta\Delta}$ that cancels out the δ-function piece from the π-exchange potential.

2. Inclusive spectra of the $^{12}C(p,n)$ reaction

In Fig. 7 we show the calculated inclusive cross section for the 0° spectrum of the ^{12}C(p,n) reaction in com-

TABLE I. The optical potential parameters used in the DWIA calculations.

	V	r	a	W	r_I	a_I
p	4.70	0.900	0.530	-30.0	0.931	0.568
n	-3.27	1.125	0.976	-25.0	1.125	0.592
^{3}He	4.70	0.900	0.530	-77.0	0.931	0.568
t	-3.27	1.125	0.976	-40.0	1.125	0.592

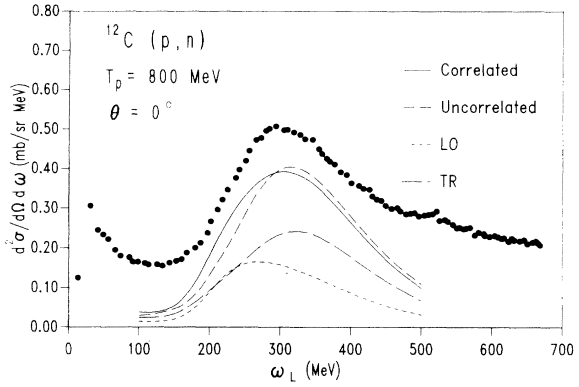

FIG. 7. Zero degree neutron spectra for the reaction ^{12}C(p,n) at E=800 MeV [5]. (a) The theoretical spectra are calculated with (full curve) or without (long-dashed curve) ph correlations. The longitudinal (LO) and transverse (TR) cross sections are also shown separately for the case where correlations are included.

parison with the experimental data. The solid and long-dashed curves represent the cross sections calculated with and without inclusion of $V_{\rm ph}$, respectively. We shall call these curves the correlated ($V_{\rm ph} \neq 0$) and uncorrelated ($V_{\rm ph} = 0$) results. The theoretical cross sections underestimate the data by a factor of N=1.3. This is due to the fact that the Δ resonance is located on top of a large continuum (background). The background is the result of various processes, the significance of which varies with excitation energy. On the high energy side of the resonance ($\omega_L \geq 350$ MeV) the background is mainly produced by projectile excitation where the proton is excited to a Δ^+ which subsequently decays into a $n+\pi^+$. At very high ω_L (≥ 500 MeV) a large fraction of the neutron cross section can be ascribed to neutrons resulting from the quasifree decay of the Δ in the target. The missing cross section on the low energy side of the Δ resonance ($\omega_L \leq 200$ MeV), i.e., in the so called "dip" region, may be due to two-step processes, two-body exchange currents, and projectile excitations [13].

The essential result in Fig. 7 is the strong energy shift between the LO (short-dashed curve) and TR (dash-dotted curve) cross sections. While the former cross section has its peak at $\omega_L \sim 260$ MeV, the latter has its peak at $\omega_L \sim 325$ MeV. The relative energy shift of ~ 65 MeV between the two peaks is an effect of the strongly attractive π-exchange interaction in the LO channel. The mechanism for this shift will be explained in detail in the next section. Note that the TR cross section is roughly twice as large as the LO cross section. This is an effect of $t_{NN,N\Delta}$ which produces a cross section ratio of TR/LO=2/1. As a result of this ratio, the large shift of ~ 65 MeV in the LO cross section leads only to a relatively small energy shift of ~ 30 MeV in the inclusive spectrum. This can be seen from a comparison of the correlated and uncorrelated results in Fig. 7.

The theoretical description of the experimental spectra at other scattering angles is also reasonably good. This can be seen from Fig. 8, where we compare the theoretical ^{12}C(p,n) cross sections with data at scattering

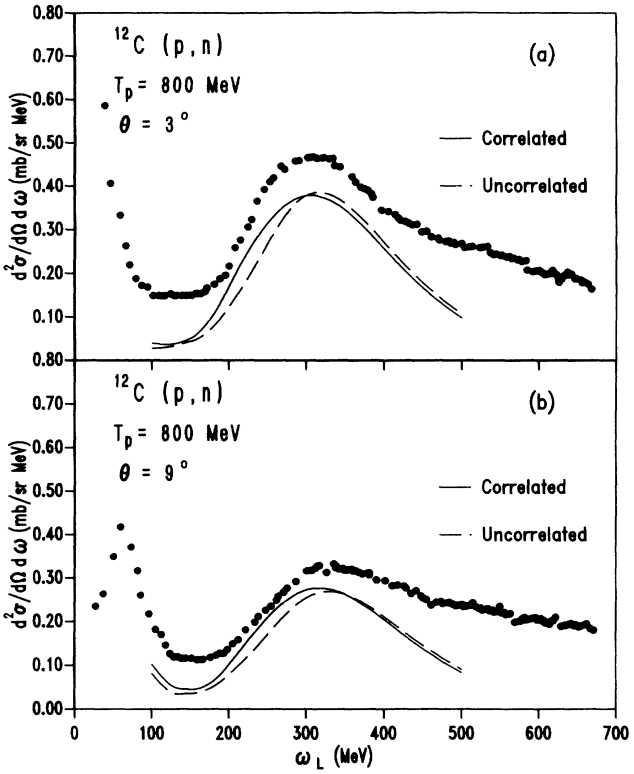

FIG. 8. Neutron spectra for the reaction ^{12}C(p,n) at E=800 MeV at scattering angles of $\theta = 3°$ (a) and $\theta = 9°$ (b). The data are taken from Ref. [5].

angles of $\theta = 3°$ and 9°. Both the shape and the magnitude of the data are reproduced well. The peak position and magnitude of the experimental cross sections change with angle. This behavior is reproduced very well by our calculations.

3. *Inclusive spectra of the ^{12}C(^{3}He,t) reaction*

The main features of the Δ excitations described above for the ^{12}C(p,n) reaction can also be found in the ^{12}C(^{3}He,t) reaction. Important differences between the two reactions, however, arise from the finite size of the projectile and the different projectile distortion. In the ^{12}C(^{3}He,t) reaction the projectile form factor (shown in Fig. 5) causes a trivial shift of the Δ peak position towards lower excitation energies. This is demonstrated in Fig. 9 by a comparison of the full and the long-dashed curves. The latter is calculated for a point projectile, i.e., neglecting the projectile form factor. The inclusion of the form factor cuts off the high energy part of the spectrum. The relative energy shift of ~ 40 MeV between the Δ peak positions of the (p,n) and (^{3}He,t) data (compare Figs. 7 and 9) is a result of this effect.

The effect of the projectile distortion on the calculated spectrum is also shown in Fig. 9. The full and short-dashed curves represent DWIA and plane wave impulse approximation (PWIA) calculations, respectively. The two theoretical cross sections differ in magnitude, but agree in shape. This means that the distortions at inter-

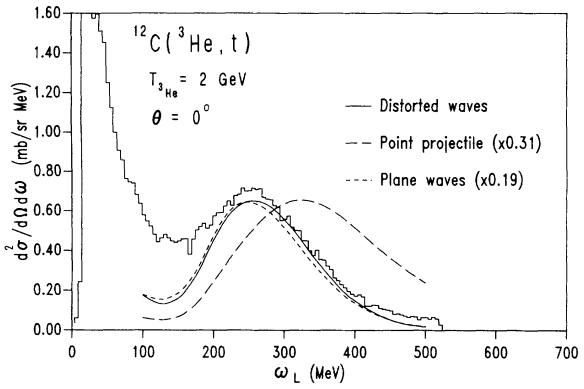

FIG. 9. Zero-degree triton spectra for the reaction ^{12}C(^{3}He,t) at E= 2 GeV. The data are taken from Ref. [2]. The theoretical spectra are calculated with (full curve) or without (long-dashed curve) ph correlations. The long-dashed line is the cross section calculated with a point projectile. The latter cross section was multiplied by 0.31.

mediate incident energies mainly lead to a pure absorption of flux, reducing the magnitude of the cross section but leaving the shape of the cross section unchanged. If there is at all an effect of distortions on the resonance shape, then it is a small upward energy shift of the DWIA cross section relative to the PWIA result.

In Fig. 10 we compare the theoretical cross sections for the ^{12}C(^{3}He,t) reaction at $\theta = 0°$ with the experimental data. The solid curve represents the cross section with inclusion of $V_{\rm ph}$, finite size effects of the projectile, and the distortion effects. We call this curve the correlated result. The long-dashed curve represents the corresponding uncorrelated result. Also the LO and TR cross sections are shown separately. In analogy to the ^{12}C(p,n) reaction, the LO cross section (short-dashed curve) peaks again at $\omega_L \sim$ 240 MeV. The TR cross section (dash-dotted curve), however, peaks now 40 MeV lower in energy than in the (p,n) case, namely at $\omega_L \sim$ 285 MeV. This is an effect of the ^{3}He-t form factor which reduces the magnitude of the TR spectrum at high excitation energies because of its exponential falloff with $\sqrt{-t}$. The shape of the LO spectrum is also affected by this, but less strongly.

It is remarkable that the calculation including the correlations reproduces the higher ω part of the ^{12}C(^{3}He,t) spectrum very well. This is due to the fact that, in contrast to the ^{12}C(p,n) reaction, there is no background on the high energy side of the resonance in the ^{12}C(^{3}He,t) reaction. In the latter reaction there is little cross section from projectile excitation, since the probability that the excited projectile decays to the triton ground state plus a pion is small. Similarly, only few tritons are expected from the quasifree decay of the target.

We remark that our calculation for the ^{12}C(^{3}He,t) reaction, as for the ^{12}C(p,n) reaction, fails to describe the cross section in the lower ω region (in the dip region). This underestimation may be ascribed to background components resulting from other reaction mechanisms than the one-step process. It is possible to extract some qualitative information on this background from the experimental data. In Fig. 11 we compare the data [2] of the ^{12}C(^{3}He,t) reaction at $\theta = 0^0$ for three different incident energies of E=1.5, 2.0, and 2.3 GeV. As seen, the cross section in the Δ resonance region increases rather dramatically with E. In contrast, the cross section below $\omega_L \sim$150 MeV remains essentially unchanged. The calculated spectra describe the data in the Δ resonance region very well, in particular the incident energy (E) dependence.

The analysis of the data indicates that the excitation mechanisms below and above $\omega_L \sim$ 150 MeV are different. In our view the reaction mechanisms involved at ω <150 MeV are due to two-step and multistep nucleon knockout processes. This conjecture receives further support by the fact that the cross section below ω <150 MeV is proportional to the mass number A, while the cross section in the Δ resonance region is proportional to $(3Z+N)$ [2] (where Z and N are the proton and neutron number of the target). The $3Z+N$ dependence of the cross section is a characteristic feature of the Δ excitation coming from the fact that the cross section of the $p+p \to n+\Delta^{++}$ process is three times larger than that for the $p+n \to n+\Delta^{+}$ process. Such a characteristic fea-

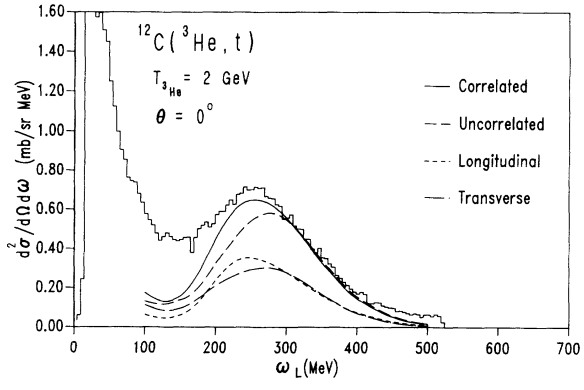

FIG. 10. Zero-degree triton spectra for the reaction ^{12}C(^{3}He,t) at E=2 GeV. The data are taken from Ref. [2]. The full curve represents the final result. In addition, the longitudinal (LO) and transverse (TR) cross sections are shown separately.

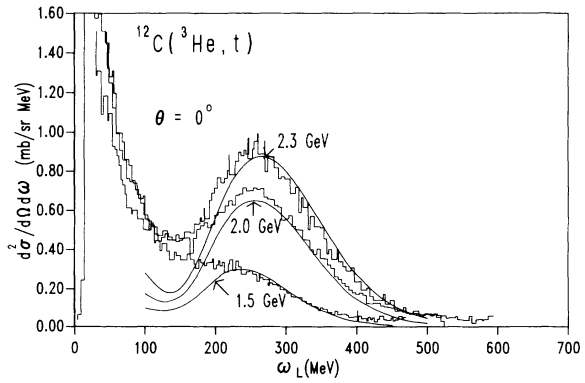

FIG. 11. Zero-degree spectra for the ^{12}C(^{3}He,t) reaction at E= 1.5, 2.0, and 2.3 GeV. The data are taken from Ref. [2]. The full curves represent the calculated cross sections including ph correlations.

ture is not seen in the cross sections below $\omega \approx 150$ MeV, indicating that the (virtual) Δ excitations do not play a significant role there.

In Fig. 12 we compare the theoretical cross section for the ^{12}C(^{3}He,t) reaction with the experimental data at other scattering angles. Although the magnitude of the cross sections changes rather dramatically with angle, this behavior is rather well reproduced by our calculations.

C. Explanation for the energy shift of the Δ resonance peak position in nuclei

In order to explain the origin of the energy shift in the spin-LO spectrum (see Figs. 7 and 9) we first perform a multipole decomposition of the inclusive cross section. In Figs. 13(a) and 13(b) we show the various partial cross section contributions σ_{J^π} corresponding to unnatural (a) and natural (b) parity states J^π, respectively. One immediately recognizes that the cross section contributions of the unnatural parity states are lowered in excitation energy by $\sim$ 60 MeV relative to those of the natural parity ones. This is due to the fact that the pion couples strongly to the unnatural parity (pionlike) states, but not to the natural parity states. Among the unnatural parity states the lower spin states undergo the bigger energy shift. This observation can be brought to a more quantitative level by explicitly calculating the energy shift

$$\Delta E_{J^\pi} = \langle \widetilde{\psi_{J^\pi}} \mid V_{\rm ph} \mid \psi_{J^\pi} \rangle \tag{71}$$

for each given state $|\psi_{J^\pi}\rangle$. Here $|\psi_{J^\pi}\rangle$ denotes the partial wave component of the continuum wave function $|\Psi\rangle$ of Eq. (23) and is normalized according to $\langle \widetilde{\psi_{J^\pi}} \mid \psi_{J^\pi} \rangle = 1$. Note that ΔE_{J^π} defined above is complex; the real part $\Delta E^R_{J^\pi}$ describes the energy shift, while the imaginary part $\Delta E^I_{J^\pi}$ describes the width associated with the coherent pion production process, as discussed already in Sec. II F.

In Figs. 14(a) and 14(b) we show the real part $\Delta E^R_{J^\pi}$ of the complex energy shift for natural and unnatural parity states, respectively. While the energy shift of the natural parity states is slightly repulsive (about +5 MeV), it is strongly attractive (about -50 MeV or so) for the unnatural parity states. In addition, in the latter case $|\Delta E^R_J|$ is large for small J, and decreases rather rapidly as J increases. Here the π-exchange interaction plays an essential role. To explain this in more detail, we show in Fig. 15(a) the momentum (q) dependence of the real part of $V_{\rm ph}$ in the LO channel (full curve) at $\omega = 250$ MeV. In addition, we show the square of two typical transition densities with $J^\pi = 1^+, L = 0$ (dashed curve) and

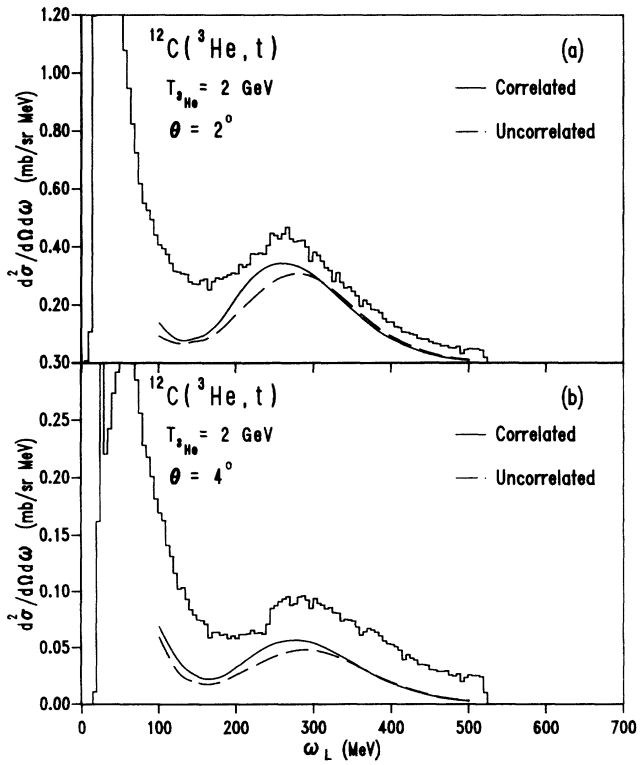

FIG. 12. Triton spectra for the reaction ^{12}C(^{3}He,t) at scattering angles of $\theta = 2°$ and of $\theta = 4°$. The data are taken from Ref. [2]. The theoretical spectra are calculated with (full curve) or without (dashed curve) ph correlations.

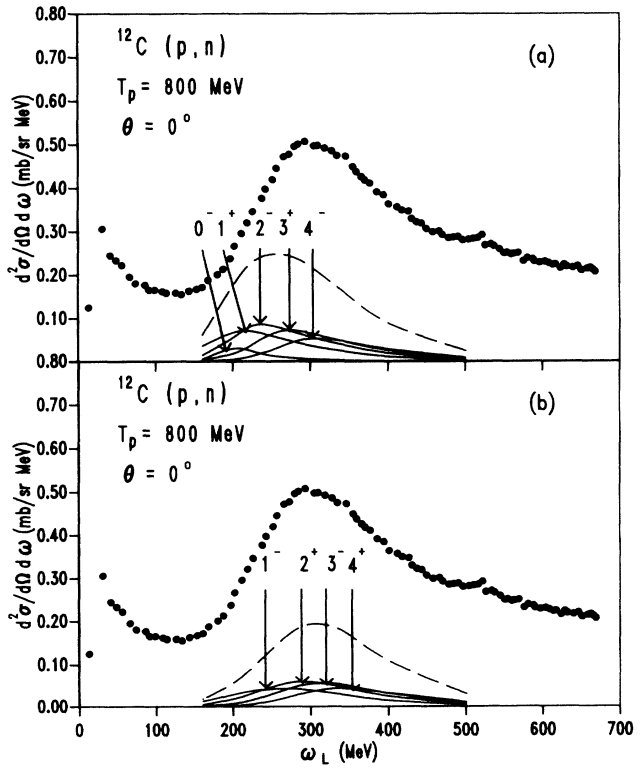

FIG. 13. Zero-degree neutron spectra for the reaction ^{12}C(p,n) at E=800 MeV [5]. (a) The cross section contributions of different unnatural parity multipoles J^π. The dashed curve represents the sum of these multipoles. (b) The cross section contributions of different natural parity multipoles J^π. The dashed curve represents the sum of these multipoles. The cross sections of the natural parity states have been scaled by a factor N=2.

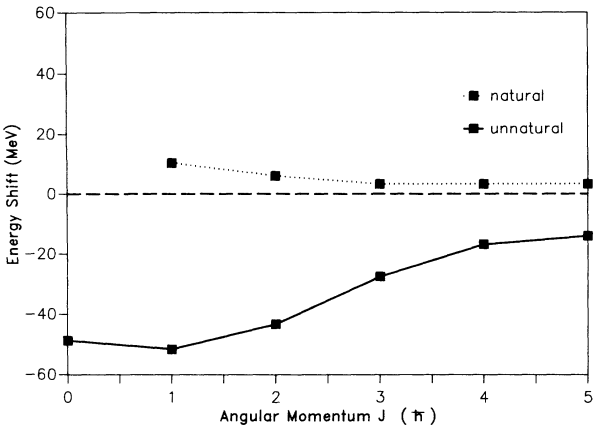

FIG. 14. The real part of the energy shift $\Delta E^R_{J^\pi}$ as function of the multipole J^π.

$J^\pi = 5^+, L = 4$ (dash-dotted curve), respectively. The square of the transition density is defined by

$$M_{\rm LO}(q) = \int d\hat{\mathbf{q}} \langle \widetilde{\psi_J} \mid \exp(-i\mathbf{q}\cdot\mathbf{r})\, \mathbf{S}^\dagger \cdot \hat{\mathbf{q}}\, T^\dagger_{\mu=-1} \mid 0\rangle \times \langle 0 \mid -T_{\mu=+1}\, \mathbf{S}\cdot\hat{\mathbf{q}}\, \exp(i\mathbf{q}\cdot\mathbf{r}') \mid \psi_J\rangle \quad (72)$$

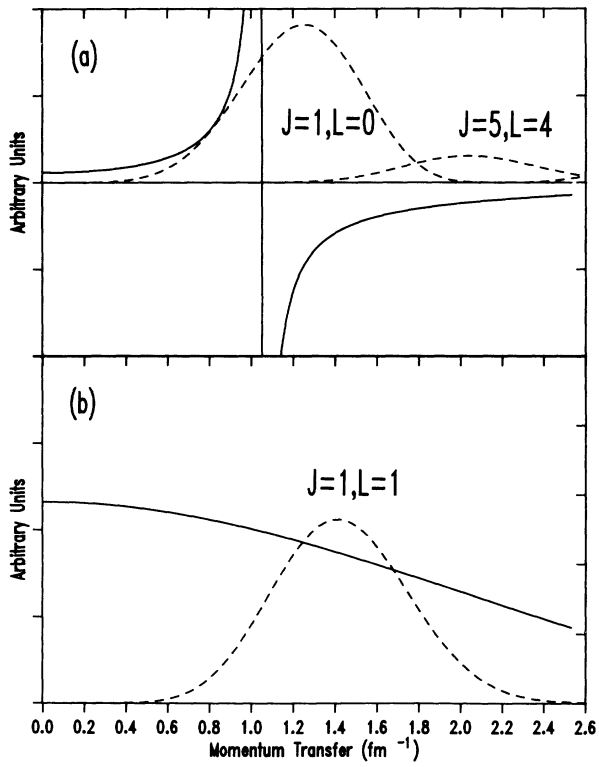

FIG. 15. The ΔN^{-1} residual interactions at $\omega = 250$ MeV as functions of momentum transfer q. (a) The full curves represent the real part of the interaction in the LO channel. The dashed and dash-dotted curves show the longitudinal transition densities with quantum numbers $J^\pi = 1^+, L = 0$ and $J^\pi = 5^+, L = 4$, respectively. (b) The full curve represents the real part of the interaction in the TR channel. The transition density with quantum numbers $J^\pi = 1^-, L = 1$ (dashed curve) is also shown.

and enters into the calculation of the energy shift as

$$\Delta E_{J^\pi} \equiv \langle \widetilde{\psi_{J^\pi}} \mid V_{\rm ph} \mid \psi_{J^\pi}\rangle = \frac{1}{(2\pi)^3} \int dq\, q^2 [V^{\rm LO}_{\rm ph}\, M_{\rm LO}(q) + V^{\rm TR}_{\rm ph}\, M_{\rm TR}(q)\,]. \quad (73)$$

Here we have split the energy shift into LO and TR components. The expression for $M_{\rm TR}(q)$ is obtained from $M_{\rm LO}(q)$ by replacing $(\mathbf{S}\cdot\hat{\mathbf{q}})$ by $(\mathbf{S}\times\hat{\mathbf{q}})$. From Fig. 15(a) one observes that $V^{\rm LO}_{\rm ph}$ has a singularity at $q_{\rm pole} = \sqrt{\omega^2 - m_\pi^2} \approx 1.05$ fm^{-1}. $V^{\rm LO}_{\rm ph}$ is repulsive for $q < q_{\rm pole}$, but attractive for $q > q_{\rm pole}$. In the charge exchange reactions the Δ in the spin-LO channel is excited by virtual π exchange. The three-momentum $|\,\mathbf{q}\,|$ carried by the virtual π is always larger than $q_{\rm pole} = \sqrt{\omega^2 - m_\pi^2}$. Thus the transition density for the Δ creation has its peak always at a momentum $q > q_{\rm pole}$. The peak of the transition density moves toward larger momentum transfers with increasing spin J^π. This can be seen by a comparison of the $J^\pi = 1^+$ and $J^\pi = 5^+$ transition densities in Fig. 15(a). From Fig. 15(a) it is then obvious that by folding $V^{\rm LO}_{\rm ph}$ with $q^2 M_{\rm LO}(q)$ a net attractive energy shift is obtained. This happens for all multipoles in the LO channel, leading to the downward energy shift of the Δ peak position. The lower the multipolarity J^π of the state is, the larger the attraction is.

In Fig. 15(b) we show a similar study for the spin-TR channel. $V^{\rm TR}_{\rm ph}$ is repulsive and has no singularity. Therefore by folding $V^{\rm TR}_{\rm ph}$ with $q^2 M_{\rm TR}(q)$ a moderate, repulsive energy shift is obtained.

D. Partial cross sections

In Sec. II F we discussed the decomposition of the total strength function S into the five components $S_{\rm KO}$, $S_{\rm KF}$, $S_{\rm QF}$, $S_{\rm SP}$, and $S_{\rm CPP}$. The corresponding partial cross sections σ_α ($\equiv d^2\sigma_\alpha/dEd\Omega$) are given by Eq. (54). Among these partial cross sections, $\sigma_{\rm KO}$ and $\sigma_{\rm KF}$ are rather small in the Δ resonance region. Therefore, in the following discussion we shall ignore $\sigma_{\rm KO}$ and $\sigma_{\rm KF}$ and concentrate on the other three partial cross sections $\sigma_{\rm SP}$, $\sigma_{\rm QF}$, and $\sigma_{\rm CPP}$.

In Fig. 16 we show the three partial cross sections as well as the summed singles cross section for the ^{12}C(p,n) reaction. In Fig. 17 we show the corresponding results for the ^{12}C(^{3}He,t) reaction. In both cases $\sigma_{\rm QF}$ gives the largest contribution to the singles cross section, explaining roughly 60% of it, while $\sigma_{\rm SP}$ and $\sigma_{\rm CPP}$ contribute 30% and 10%, respectively. Note that $\sigma_{\rm SP}$ and $\sigma_{\rm CPP}$ are peaked at energies roughly 100 MeV lower than $\sigma_{\rm QF}$. The shift of $\sigma_{\rm CPP}$ is mainly produced by the pionic mode in the LO channel [see also Fig. 18(c) below]. The large shift of $\sigma_{\rm SP}$ relative to $\sigma_{\rm QF}$ is somewhat surprising, but it can be understood from the fact that the main contribution to $\sigma_{\rm SP}$ comes from the nuclear interior where $W_\Delta(r)$ has an appreciable value. The calculations show that the low spin states give a relatively large contribution to $\sigma_{\rm SP}$. This is interesting since, as seen in Fig. 13, the peaks of

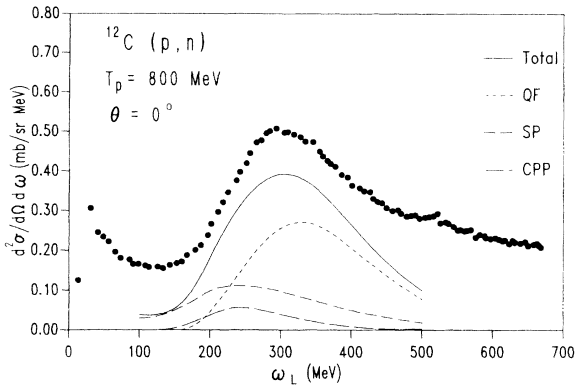

FIG. 16. Decomposition of the zero-degree singles cross section into partial cross sections for the ^{12}C (p,n) reaction at E=800 MeV. The different cross section contributions are due to quasifree Δ decay (QF), Δ spreading (SP), and coherent pion production (CPP).

the spectra of lower spin states are shifted down to lower energies.

In order to further study the correlation effect on the partial cross sections, we decompose them according to LO and TR excitations, taking the ^{12}C(p,n) reaction as an example. In Figs. 18(a)–(c) we show the LO and TR components of $\sigma_{\rm QF}$, $\sigma_{\rm SP}$, and $\sigma_{\rm CPP}$, respectively. The TR part of $\sigma_{\rm QF}$ in Fig. 18(a) peaks at about the same position as the uncorrelated spectrum in Fig. 7, indicating that no correlations are involved in this part of the spectrum. However, the LO part of $\sigma_{\rm QF}$ peaks at a lower ω_L by about 30 MeV than the TR part, indicating that even in the QF production events there are some correlation effects through the correlated wave function $|\psi\rangle$. Note that the TR/LO ratio of $\sigma_{\rm QF}$ is approximately 2, as expected from the TR/LO ratio of the $t_{NN,N\Delta}$ operator in Eq. (10).

The TR/LO ratio, however, strongly deviates from 2 in $\sigma_{\rm SP}$, as seen in Fig. 18(b), and this is due to the correlation effects in the LO channel. As already remarked, the main contribution to $\sigma_{\rm SP}$ comes from lower spin states, in which more correlations are involved. Therefore, the effects of the correlation appear in a more dramatic manner in $\sigma_{\rm SP}$ than in $\sigma_{\rm QF}$.

Figure 18(c) shows that the coherent pion production cross section $\sigma_{\rm CPP}$ is dominated by the LO component. The cross section peaks at an excitation energy of ω_L =250 MeV. This is in line with the peak position of the LO cross section in Fig. 7. An interesting aspect here is that the TR spectrum peaks at ω_L=230 MeV, which is even lower than the peak of the LO spectrum. This is an effect of the nuclear form factor, as will be explained in Sec. III E, where calculations of the triple differential cross section for CPP are presented. The comparison of

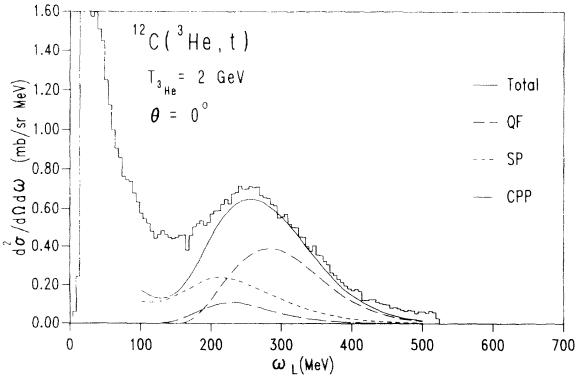

FIG. 17. Decomposition of the zero-degree singles cross section into partial cross sections for the ^{12}C(^{3}He,t) reaction at E=2 GeV. The different cross section contributions are due to quasifree Δ decay (QF), Δ spreading (SP), and coherent pion production (CPP).

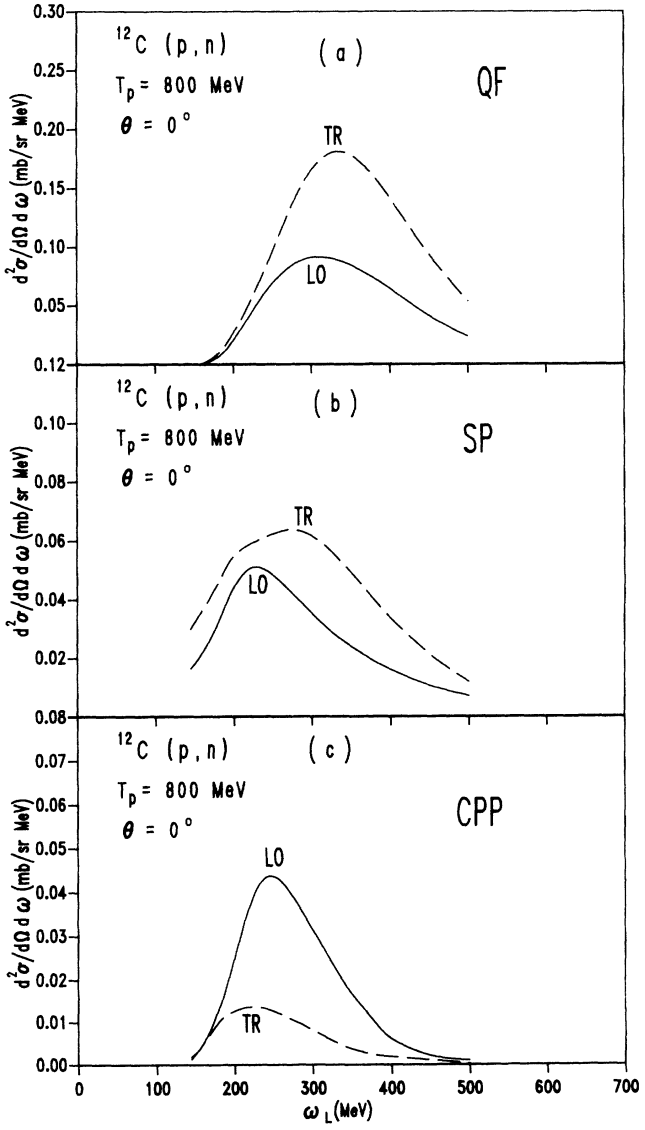

FIG. 18. Decomposition of the zero-degree singles cross section into partial cross sections in case of the ^{12}C(p,n) reaction at E=800 MeV. (a) The QF cross section separated for LO and TR excitation. (b) The SP cross section separated for LO and TR excitation. (c) The CPP cross section separated for LO and TR excitation.

the calculated CPP cross section with experiment will also be made there.

E. Exclusive differential cross sections for coherent pion production

In order to obtain more concrete evidence for the coherent mode, exclusive cross section data have been taken for the $^{12}C(p,n\pi^+)$ [20] and $^{12}C(^3He,t\pi^+)$ [21,22] reactions. In Fig. 19 we compare the calculated $^{12}C(p,n\pi^+)^{12}C(g.s.)$ coincidence cross section (dotted curve) with the measured data of Chiba *et al.* [20]. The calculations were done by integrating the triple differential cross section of Eq. (61) over the pion angle in the acceptance range of $12° \leq \theta \leq 141°$ of the detector [20]. The theoretical cross section somewhat underestimates the data, and also the calculated peak position of E_π= 250 MeV is lower than the experimental one. Note, however, that the experimental cross section includes not only contributions from real CPP events, but also from false events, such as those of the $^{12}C(p,n\pi^+n)$ and $^{12}C(p,n\pi^+p)$ reactions where the neutron or proton escapes the experimental detection [20]. An additional contribution to the pion cross section may also come from projectile excitation events, where the projectile is excited to a Δ^+ which decays into $n+\pi^+$. In Fig. 19 we show among others the contribution from the $^{12}C(p,n\pi^+n)$ reaction (dashed curve). The calculated cross section of this reaction has its peak at much higher excitation energy ($\omega_L \sim$ 350 MeV) than the cross section of the CPP process. This additional contribution, if added, leads to an improvement of the fit to the data (full curve). Further improvements will be obtained if one adds the contributions from the other processes (or if one subtracts the false events from the data). An example of this will be seen below in the analysis made for the $^{12}C(^3He,t\pi^+)^{12}C(g.s.)$ reaction.

In Fig. 20 we compare the calculated $^{12}C(^3He,t\pi^+)^{12}C(g.s.)$ (pion angle integrated) coincidence cross section with the measured data of Hennino *et al.* [22]. In this measurement [22] events with tritons emitted into the angular range between 2.5° and 3.5° and with an energy window of 50 MeV around the target ground state were taken. Because of this choice of the triton emission angle, the contribution of the false events from the $^{12}C(^3He,t\pi^+p)$ reaction is strongly suppressed. Also, the contribution from the projectile excitation is expected to be small for this reaction. The data are remarkably well reproduced by the calculated coincidence cross section. We note particularly that the calculation reproduces fairly well the magnitude of the CPP cross section in relation to that of the singles; in fact the observed ratio of the peak cross section of CPP to singles is 0.12 [22], while the calculated ratio is 0.11.

In Fig. 21 we compare the calculated pion angular distribution obtained by integrating the triple differential cross section over the triton energy with the data [22]. The contributions from the LO and TR channels to the calculated cross section are also shown separately.

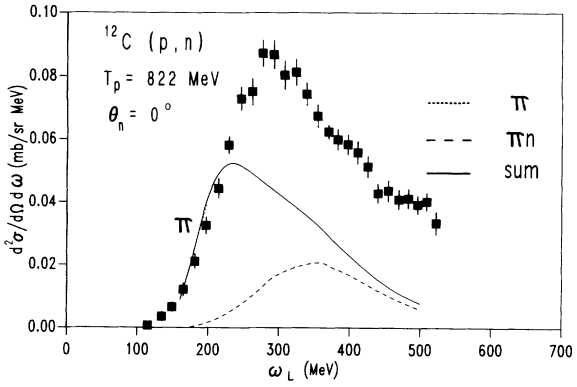

FIG. 19. Pion coincidence spectrum for the $^{12}C(p,n)$ reaction at E=822 MeV. The data are taken from Ref. [20]. The data are compared to the calculated zero-degree coherent pion production cross section (dotted curve) and to the π^+n coincidence (dashed curve) cross section. The sum of both cross sections is represented by the full curve.

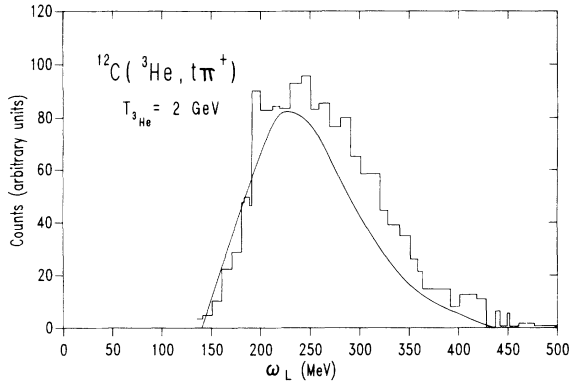

FIG. 20. Pion coincidence spectrum for the $^{12}C(^3He,t)$ reaction at E=2 GeV in comparison with the data of Hennino *et al.* [22].

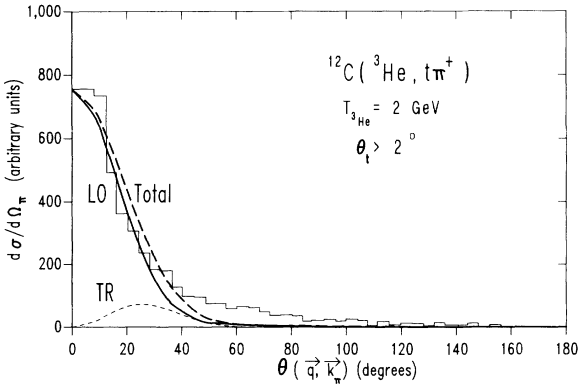

FIG. 21. Count rate of the $^{12}C(^3He,t\pi^+)$ reaction as function of $\theta(\mathbf{q},\mathbf{p}_\pi)$, which is the angle between the outgoing π^+ and the momentum transfer $\mathbf{q}$. The data are taken from Hennino *et al.* [22]. The theoretical angular distribution is represented by the full curve. The angular distributions for spin-LO (long-dashed curve) and spin-TR (short-dashed curve) excitation are also shown separately.

For the sake of comparison, we have normalized the final theoretical cross section to the experimental count rates at $\theta_\pi = 0°$. Note that the angle θ_π is measured from the direction of the momentum transfer $\mathbf{q}$. The calculated cross section fits to the experimental cross section very well. The shape of the LO angular distribution is strongly forward peaked, which means that most of the pions are emitted into the direction of the momentum transfer $\mathbf{q}$. This forward peaked character is partially explained in terms of the spin structure of the excitation ($\mathbf{S}^\dagger \cdot \mathbf{q}$) and deexcitation ($\mathbf{S} \cdot \mathbf{k}_\pi$) operators involved in the pion production through the spin-LO channel. The product of these two operators gives rise to a factor $qk_\pi \cos\theta_\pi$ in the resultant transition amplitude and thus a factor $\cos^2\theta_\pi$ in the cross section. This factor peaks at $\theta_\pi = 0°$. As seen, however, both the calculated and the experimental angular distributions are much more strongly forward peaked than the $\cos^2\theta_\pi$ factor predicts. An important additional angular-dependent factor comes, however, from the radial overlap integral in Eq. (60). This overlap integral becomes larger as the scattering angle θ_π gets smaller. This is due to the dependence of the integral on the recoil momentum $\mid \mathbf{q} - \mathbf{p}_\pi \mid$ transferred to the target in the coherent π decay process. This recoil momentum is smallest for $\mathbf{q}$ parallel with $\mathbf{p}_\pi$, making the overlap integral largest for θ_π=0°.

It is important to note that the angular distribution of the LO component is very similar to that of the pion elastic scattering. This suggests that there is a close relation between the LO coherent pion production on the one hand and elastic pion-nucleus scattering on the other. In fact, we may view the coherent pion production process as a kind of elastic scattering process, in which an initially off-mass-shell pion with the momentum $\mathbf{q}$ is converted into an on-mass-shell pion by the multiple scattering in the nucleus. This conversion process is possible since the target nucleus as a whole can provide the extra momentum needed to put the pion on its mass shell. In the ^{12}C(^{3}He,$t\pi^+$)^{12}C(g.s.) reaction the recoil momentum amounts to $\Delta q \approx 0.5$ fm^{-1} at $\omega_L = 250$ MeV corresponding to a recoil energy of $\Delta\omega_L \leq 1$ MeV for the ^{12}C nucleus.

In Fig. 21 we also show the TR angular distribution. This angular distribution has again a characteristic shape with a minimum at $\theta_\pi = 0°$ and a maximum at $\theta_\pi \approx 30°$. This shape is very similar to that of angular distributions observed in pion photoproduction (γ, π) reactions [48–50] and pion electroproduction [51–53]. The spin structure of the excitation ($\mathbf{S} \times \mathbf{q}$) and deexcitation ($\mathbf{S}^\dagger \cdot \mathbf{k}_\pi$) operators involved in (γ, π) reactions is exactly the same as that of the TR excitation of the nucleus by (p, n) reactions. The product of both operators makes the angular distribution proportional to $\mid \mathbf{q} \times \mathbf{k}_\pi \mid^2 = (qk_\pi \sin\theta_\pi)^2$. This product vanishes for θ_π=0° and peaks for θ_π=90°. As discussed above, there is, however, an additional effect coming from the overlap integral, which makes the resultant angular distribution more forward peaked. Note that the magnitude of the TR cross section is small in comparison to that of the LO cross section. This is again an effect of the overlap integral which decreases rapidly with increasing momentum transfer. This is also responsible for the fact that in Fig. 18(c) the peak of the TR energy spectrum appears at a lower ω_L than that of the LO spectrum.

F. Spin observables in the ^{12}C(p, n) reaction

The calculated spin transfer coefficients for the 800 MeV ^{12}C(p, n) reaction are shown in Fig. 22. Here the observables D_{xx} and D_{zz} calculated with inclusion of ph correlations (full curves) are compared with the uncorrelated results (dashed curves). A large effect due to the correlations is seen in both quantities. It is thus highly desirable to measure the coefficients D_{xx} and D_{zz}.

We remark that at Saturne in Saclay an experiment with similar motivation looking for the spin-LO correlation effect in nuclei was performed [46]. In this experiment the tensor analyzing power in the ^{12}C$(\mathbf{d}, 2p)$ reaction at $E_{\rm lab}$=2 GeV was measured [46]. We have analyzed [47] these data, finding that the data at forward angles were not reproduced very well by our calculations, particularly not in the excitation energy region where the pion correlations play an important role, i.e., at $\omega_L \sim 250$ MeV. We believe that this problem that we have in describing the data at forward angles and lower excitation energies is due to cross section contributions from other reaction mechanisms, e.g., multistep nucleon-knockout or other reaction mechanisms which destroy the information

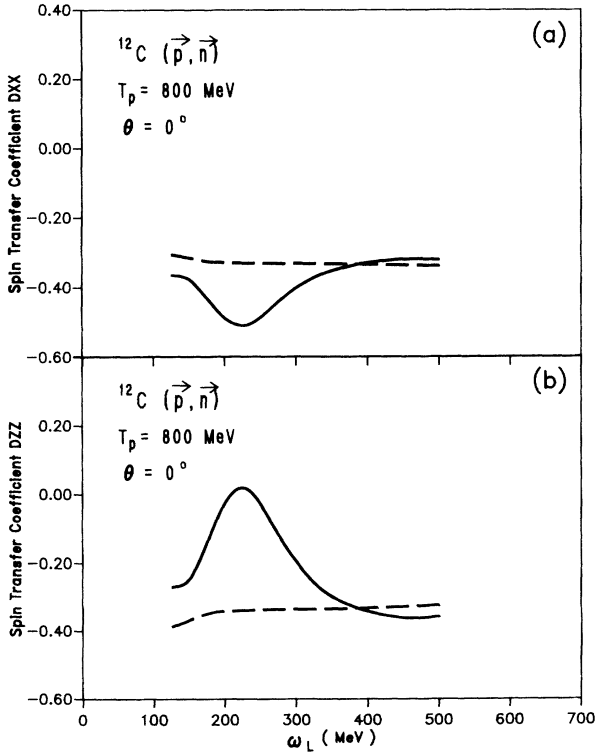

FIG. 22. Calculated spin transfer coefficients for the ^{12}C(p, n) reaction at E=800 MeV and at zero degrees. (a) D_{zz} and (b) D_{xx}. The theoretical results with and without the ΔN^{-1} correlations are shown by the full and dashed curves, respectively.

in the spin observables. Just as in the $(\mathbf{d}, 2p)$ reaction, contributions from different reaction mechanisms other than one-step Δ excitation might also contribute to the (p,n) reaction. This is particularly true for the lower ω energy region of the Δ resonance, as the observed (p,n) spectra are not reproduced here by our calculations.

IV. SUMMARY AND CONCLUSIONS

We have presented an approach to calculate the spin-isospin response function of nuclei in the Δ resonance region. Our approach treats the distortion effects on the incident projectile and outgoing ejectile properly and includes the $V_{\rm ph}$ correlations in the nucleus explicitly. When the residual ph interaction is switched on, the equations for the Δ wave functions become coupled equations. We have solved these equations by using the Lanczos method.

Results of numerical analyses are presented for the (p,n) and $(^3\mathrm{He},t)$ reactions at intermediate projectile energies. The shift of the Δ peak position observed in these reactions is shown to be due to the strongly attractive correlations in the LO spin-isospin channel. This attraction comes from the energy-dependent π-exchange interaction. To obtain sufficient attraction we need a $g'_{\Delta\Delta}$ parameter of about 1/3 (in units of $J_{\pi\Delta\Delta} = f_{\pi N\Delta} f_{\pi N\Delta}/m_\pi^2 \approx 1600$ MeV fm^3). This value corresponds to minimal short-range correlations. No significant energy shift is found in the TR channel. This is in agreement with what is observed in the electroexcitation of the Δ, e.g., in the photon-nucleus total cross section.

Furthermore, we have shown that for charge exchange reactions the pion coincidence cross section is an excellent tool for the study of the LO response function in the Δ resonance region. The peak position of the coherent pion component is significantly shifted toward lower excitation energies by the Δ hole correlations. In addition, it is shown that the pions are strongly forward (in the direction of $\hat{\mathbf{q}}$) peaked. Both effects, the energy shift and the forward peaking of coherent pions, prove that the recent SATURNE experiment has indeed identified the nuclear pionic mode [22]. A more accurate interpretation of the π^+ events requires a thorough investigation of both the angular distribution of the $p\pi^+$ events and of the π^+ events originating from projectile excitation. Such investigations are in progress.

Finally, we have pointed out that the spin transfer coefficients are a good source of information on the pion correlations in nuclei. Up to now only few data are available. We thus hope that more data, especially those with better resolution, will be accumulated in the near future.

ACKNOWLEDGMENTS

This work is supported in part by the Studienstiftung des deutschen Volkes, by the Graduiertenkolleg "Die Erforschung Subnuklearer Strukturen der Materie" at the University of Bonn, by the U.S. Department of Energy under Contract No. DE-FG03-93ER40785, and by the Ministry of Education, Korea (Project No. BSRI-93-223).

APPENDIX A: EXPLICIT FORMULA FOR THE SOURCE FUNCTION AND FOR THE MATRIX ELEMENTS OF THE PARTICLE-HOLE RESIDUAL INTERACTION

In this Appendix, we derive the formulas for the radial source function $\rho_{\rm ph}(r)$ and for the ph matrix elements $V^{j_t}_{{\rm ph},p'h'}(r',r)$. The radial source function is obtained from Eq. (28) by inversion

$$\rho_{\rm ph}(r) = \frac{1}{\sqrt{2}} \sum_{m_a m_b m_{s_t} m_{j_t}} (-1)^{1/2+m_a} \langle s_b m_b s_a - m_a \mid s_t m_{st} \rangle \times (-1)^{\ell+m_{\ell_t}} \langle j_t m_{j_t} s_t m_{s_t} \mid \ell_t m_{\ell_t} \rangle r([y_{\ell m_\ell} \Phi_h]_{j_t m_{j_t}} \mid \rho\rangle, \tag{A1}$$

where

$$\mid \rho\rangle = \sum_{j=1,A} (\phi_{s_b m_b \nu_b} \mid \sum_{i=1,a} f_{ab}(\sqrt{-t}) t_{ij}(\omega, \mathbf{q}\,) \times X_{\rm DW}(\mathbf{k}_a, \mathbf{k}_b, \mathbf{r}_j) \mid \phi_{s_a m_a \nu_a}) \mid \Phi_A\rangle. \tag{A2}$$

In the overlap matrix element of Eq. (A1) the parenthesis denotes the integration over all channel coordinates including those of the hole nucleus. To perform the integration we first make a multipole expansion of the distortion function,

$$X_{\rm DW}(\mathbf{k}_a, \mathbf{k}_b, \mathbf{r}) = \sum_{\ell m} X_{\ell m}(\mathbf{k}_a, \mathbf{k}_b, r) i^\ell Y_{\ell m}(\Omega), \tag{A3}$$

with

$$X_{\ell m}(\mathbf{k}_a, \mathbf{k}_b, \mathbf{r}) = (\chi_b^{(-)} \mid i^\ell Y_{\ell m} \mid \chi_a^{(+)}). \tag{A4}$$

Now we write the effective interaction t_{ij} in terms of central (C) and tensor (T) components,

$$t_{ij} = \sum_{k=0,2} V_k(\omega, q) Y_k(\hat{\mathbf{q}}) \cdot [\boldsymbol{\sigma}_i \times \boldsymbol{\mathcal{S}}_j]^{(k)}, \tag{A5}$$

where

$$V_k(\omega, q) = \begin{cases} \sqrt{12\pi} V_C(\omega, q) & \text{if } k = 0, \\ -\sqrt{\frac{24\pi}{5}} V_T(\omega, q) & \text{if } k = 2. \end{cases} \tag{A6}$$

Insertion of Eq. (A2) with (A3)–(A6) into Eq. (A1) leads after some lengthy angular momentum algebra to

$$\rho_{\rm ph}(r) = \sqrt{2} f_{ab}(\omega, \mathbf{q}) \sum_{k,\ell} \hat{k}\hat{j}_t W(\ell\ell_t 11; kj_t) \times V_k(\omega, q)[X_\ell Y_k]_{\ell_t m_{\ell_t}} g_{\ell j_t}(ph) r u_h(r), \quad \text{(A7)}$$

where the ph angular momentum matrix element is reduced in spin and isospin space and is given by

$$g_{\ell j}(ph) = \hat{j}^{-1} \langle p \,||\, i^\ell [Y_\ell \mathcal{S}]_j \mathcal{T}_- \,||\, h \rangle. \quad \text{(A8)}$$

The evaluation of $V^{j_t}_{p_1h_1,p_2h_2}(r_1, r_2)$ starts from its definition in Eq. (30). First we transform the ph interaction into coordinate space,

$$V_{\rm ph}(\mathbf{x}) = \int d^3\mathbf{q} \, \exp\{i\mathbf{x}\cdot\mathbf{q}\} V_{\rm ph}(\mathbf{q}). \quad \text{(A9)}$$

A multipole expansion with respect to the coordinates $\mathbf{r}_1$ and $\mathbf{r}_2$ gives ($x = |\, \mathbf{r}_1 - \mathbf{r}_2 \,|$)

$$V_{\rm ph} = -(\mathcal{T}\cdot\mathcal{T}^\dagger) \sum_{\ell_1\ell_2 jm} v_{\ell_1\ell_2 j}(r_1, r_2) [i^{\ell_1} Y_{\ell_1} \otimes \mathcal{S}_1]_{jm} \times [i^{\ell_2} Y_{\ell_2} \otimes \mathcal{S}_2]_{j\tilde{m}}, \quad \text{(A10)}$$

where

$$v_{\ell_1\ell_2 j}(r_1, r_2) = -4\pi v^C_{\ell_1\ell_2}(r_1, r_2)\delta_{\ell_1\ell_2} + 4\pi\sqrt{6}(-1)^j \hat{\ell}_1\hat{\ell}_2 \langle \ell_1 0 \ell_2 0 \mid 20\rangle \times W(\ell_1 1 \ell_2 1; j2) v^T_{\ell_1\ell_2}(r_1, r_2). \quad \text{(A11)}$$

The central and tensor multipole coefficients are defined by

$$v^C_{\ell\ell}(r_1, r_2) = w^C_\ell(r_1, r_2),$$

$$v^T_{\ell\ell}(r_1, r_2) = \frac{2\ell+3}{2\ell+1} r_1 r_2 w^T_{\ell-1}(r_1, r_2)(r_1^2 + r_2^2) \times w^T_\ell(r_1, r_2) + \frac{2\ell-1}{2\ell+1} r_1 r_2 w^T_{\ell+1}(r_1, r_2),$$

$$v^T_{\ell-1\ell+1}(r_1, r_2) = r_2^2 w^T_{\ell-1}(r_1, r_2) - 2 r_1 r_2 w^T_\ell(r_1, r_2) + r_1^2 w^T_{\ell+1}(r_1, r_2), \quad \text{(A12)}$$

$$v^T_{\ell+1\ell-1}(r_2, r_1) = v^T_{\ell-1\ell+1}(r_1, r_2),$$

where

$$w^C_\ell(r_1, r_2) = \frac{1}{2}\int V_C(r) P_\ell(\mu) d\mu, \quad \text{(A13)}$$

$$w^T_\ell(r_1, r_2) = \frac{1}{2}\int r^{-2} V_T(r), P_\ell(\mu) d\mu, \quad \text{(A14)}$$

and $\mu = \cos(\mathbf{r}_1, \mathbf{r}_2)$. Insertion of Eq. (A10) into Eq. (30) results in

$$V^{j_t}_{p_1h_1,p_2h_2}(r_1, r_2) = \sum_{\ell_1\ell_2} v_{\ell_1\ell_2 j_t}(r_1, r_2) r_1 u_{h_1}(r_1) g_{\ell_1 j_t}(p_1h_1) r_2 u_{h_2}(r_2) g_{\ell_2 j_t}(p_2h_2), \quad \text{(A15)}$$

where $g_{\ell j}(ph)$ has been defined already in Eq. (A8).

APPENDIX B: LANCZOS METHOD

We discuss here the Lanczos method used to solve Eq. (33). In this method we expand $|\lambda\rangle$ with a set of $N+1$ biorthogonal basic wave functions $|D_i\rangle$ ($i = 0, 1, ..., N$), which we generate iteratively as

$$|D_0\rangle = \frac{1}{N_0}|\rho\rangle, \quad \text{(B1)}$$

$$|D_{i+1}\rangle = \frac{1}{N_i}\left[\mathcal{V}\mathcal{G}_0|D_i\rangle - \sum_{j=0}^{i} |D_j\rangle\alpha_{ji}\right], \quad \text{(B2)}$$

with

$$\alpha_{ji} = \begin{cases} \langle \tilde{D}_j | \mathcal{V}\mathcal{G}_0 | D_i\rangle & \text{if } j \le i+1, \\ 0.0 & \text{if } j > i+1. \end{cases} \quad \text{(B3)}$$

N_i in Eq. (B2) is the normalization constant determined from the condition $\langle \tilde{D}_i | D_i\rangle = 1$, $|\tilde{D}_i\rangle$ being the conjugate state to $|D_i\rangle$. The coefficients α_{ji} given by (B3) are determined from the Schmidt orthonormalization procedure.

In terms of $|D_i\rangle$, $|\lambda\rangle$ is expanded as

$$|\lambda\rangle = \sum_{i=0}^{N} C_i |D_i\rangle. \quad \text{(B4)}$$

Inserting Eq. (B4) into (33) one can easily derive an inhomogeneous linear equation for the expansion coefficient C_i, i.e.,

$$\sum_j (\delta_{ij} - \alpha_{ij}) C_j = N_0 \delta_{0i}. \quad \text{(B5)}$$

The values of C_i are then determined by solving Eq. (B5). Note that Eq. (B5) can be solved rather easily, because $\alpha_{ji} = 0$ for $j > i+1$.

[1] V. G. Ableev *et al.*, Pis'ma Zh. Eksp. Teor. Fiz. **40**, 2 (1984) [Sov. Phys. JETP. Lett. **40**, 763 (1984)].
[2] D. Contardo *et al.*, Phys. Lett. B **168**, 331 (1986).
[3] C. G. Cassapakis *et al.*, Phys. Lett. **63B**, 35 (1976).
[4] B. E. Bonner *et al.*, Phys. Rev. C **18**, 1418 (1978).
[5] D. A. Lind, Can. J. Phys. **65**, 637 (1987).
[6] C. Gaarde, Annu. Rev. Nucl. Sci. **41**, 187 (1991).
[7] F. Osterfeld, Rev. Mod. Phys. **64**, 491 (1992).

[8] B. K. Jain and A. B. Santra, Nucl. Phys. **A519**, 697 (1990).
[9] H. Esbensen and T.- S. H. Lee, Phys. Rev. C **32**, 1966 (1985).
[10] J. Delorme and P. A. M. Guichon, in Proceedings of the 10th Biennale de Physique Nucleaire, Aussois, 1989, Lycen 8906 (unpublished); p. C.4.1, Phys. Lett. B **263**, 157 (1991).
[11] T. Udagawa, S. W. Hong, and F. Osterfeld, Phys. Lett. B **245**, 1 (1990).
[12] S.-W. Hong, F. Osterfeld, and T. Udagawa, in *Proceedings of the International Conference on Nuclear Collective Motion and Nuclear Reaction Dynamics*, edited by K.-I. Kubo *et al.* (World Scientific, Singapore, 1991), p. 261.
[13] E. Oset, E. Shiino, and H. Toki, Phys. Lett. B **224**, 249 (1989).
[14] P. F. de Cordoba and E. Oset, Nucl. Phys. **A544**, 793 (1992).
[15] M. Ericson, Nucl. Phys. **A518**, 116 (1990).
[16] V. F. Dmitriev and T. Suzuki, Nucl. Phys. **A438**, 697 (1985).
[17] V. F. Dmitriev, Phys. Lett. B **226**, 219 (1989); Phys. Rev. C **48**, 357 (1993).
[18] G. Chanfray and M. Ericson, Phys. Lett. **141B**, 163 (1984).
[19] J. B. McClelland *et al.*, Phys. Rev. Lett. **69**, 582 (1982).
[20] J. Chiba *et al.*, Phys. Rev. Lett. **67**, 1982 (1991).
[21] T. Hennino *et al.*, Phys. Lett. B **283**, 42 (1992).
[22] T. Hennino *et al.*, Phys. Lett. B **303**, 236 (1993).
[23] P. Oltmanns, F. Osterfeld, and T. Udagawa, Phys. Lett. B **299**, 194 (1993).
[24] F. Osterfeld, B. Körfgen, P. Oltmanns, and T. Udagawa, Phys. Scr. **48**, 95 (1993).
[25] E. Oset, P. F. de Cordoba, J. Nieves, and M. J. Vicente-Vacas, Phys. Scr. **47**, 793 (1993).
[26] T. E. O. Ericson, Nucl. Phys. **A560**, 458 (1993).
[27] M. Hirata, J. H. Koch, F. Lenz, and E. J. Moniz, Phys. Lett. **70B**, 281 (1977); Ann. Phys. (N.Y.) **120**, 205 (1979).
[28] E. Oset, H. Toki, and W. Weise, Phys. Rep. **83**, 281 (1982).
[29] T. E. O. Ericson and W. Weise, *Pions in Nuclei* (Oxford University Press, Oxford, 1988).
[30] J. Arends *et al.*, Z. Phys. A **311**, 367 (1983); Phys. Lett. **98B**, 423 (1981).
[31] P. Barreau *et al.*, Nucl. Phys. **A402**, 515 (1983).
[32] J. S. O'Connell *et al.*, Phys. Rev. Lett. **53**, 1627 (1984).
[33] R. M. Sealock *et al.*, Phys. Rev. Lett. **62**, 1350 (1989).
[34] Y. Horikawa, M. Thies, and F. Lenz, Nucl. Phys. **345A**, 386 (1980).
[35] A. K. Kerman, H. McManus, and R. M. Thaler, Ann. Phys. (N.Y.) **8**, 551 (1959).
[36] V. F. Dmitriev, O. P. Sushkov, and C. Gaarde, Nucl. Phys. **A459**, 503 (1986).
[37] L. Wolfenstein and J. Ashkin, Phys. Rev. **85**, 947 (1952).
[38] M. H. MacGregor, M. J. Moravcsik, and H. P. Stapp, Annu. Rev. Nucl. Sci. **10**, 291 (1960).
[39] J. P. Auger, C. Lazard, R. J. Lombard, and R.R. Silbar, Nucl. Phys. **A442**, 621 (1985).
[40] T. Udagawa and B. T. Kim, Phys. Rev. C **40**, 2271 (1989).
[41] P. Oltmanns, F. Osterfeld, and T. Udagawa (unpublished).
[42] J. Bystricky, F. Lehar, and P. Winternitz, J. Phys. (Paris) **39**, 1 (1978).
[43] J. M. Moss, in *Proceedings of the International Conference on Spin Excitations in Nuclei*, edited by F. Petrovich, G. E. Brown, G. T. Garvey, C. D. Goodman, R. A. Lindgren, and W. G. Love (Plenum, New York, 1984), p. 355.
[44] P. Desgrolard, J. Delorme, and C. Gignoux, Nucl. Phys. **A544**, 811 (1992).
[45] G. Glass *et al.*, Phys. Lett. **129B**, 27 (1983).
[46] C. Ellegaard *et al.*, Phys. Lett. B **231**, 365 (1989).
[47] P. Oltmanns, Ber. Forschungszent, Jülich, ISSN 0366-0885, 2510 (1991).
[48] J. H. Koch, E. J. Moniz, and N. Ohtsuka, Ann. Phys. (N.Y.) **154**, 99 (1984).
[49] T. Takaki, T. Suzuki, and J. H. Koch, Nucl. Phys. **A443**, 570 (1985).
[50] I. Laktineh, W. M. Alberico, J. Delorme, and M. Ericson, Nucl. Phys. **A555**, 237 (1993).
[51] J. H. Koch and N. Ohtsuka, Nucl. Phys. **A435**, 765 (1985).
[52] S. Hirenzaki, J. Nieves, E. Oset, and M. J. Vicente-Vacas, Phys. Lett. B **304**, 198 (1993).
[53] I. Bergqvist *et al.*, Nucl. Phys. **A469**, 648 (1987).